

# A Comparative Study of Thermodynamic, Conformational, and Structural Properties of Bottlebrush with Star and Ring Polymer Melts

Alexandros Chremos<sup>1, a)</sup> and Jack F. Douglas<sup>1, b)</sup>

Materials Science and Engineering Division, National Institute of Standards and Technology, Gaithersburg, MD, 20899, USA

(Dated: 11 July 2018)

Thermodynamic, conformational, and structural properties of bottlebrush polymer melts are investigated with molecular dynamics simulations and compared to linear, regular star and unknotted ring polymer melts to gauge the influence of molecular topology on polymer melt properties. We focus on the variation of the backbone chain length, the grafting density along the backbone, and the length of the side chains at different temperatures above the melt glass transition temperature. Based on these comparisons, we find that the segmental density, isothermal compressibility, and isobaric thermal expansion of bottlebrush melts are *quantitatively* similar to unknotted ring polymer melts and star polymer melts having a moderate number ( $f = 5$  to 6) of arms. These similarities extend to the mass scaling of the chain radius of gyration. Our results together indicate that the configurational properties of bottlebrush polymers in their melt state are more similar to randomly branched polymers than linear polymer chains. We also find that the average shape of bottlebrush polymers having short backbone chains with respect to the side chain length is also rather similar to unknotted ring and moderately branched star polymers in their melt state. As a general trend, the molecular shape of bottlebrush polymers becomes more spherically symmetric when the length of the side chains has a commensurate length as the backbone chain. Finally, we calculate the partial static structure factor of the backbone segments and we find the emergence of a peak at the length scales that characterizes the average distance between the backbone chains. This peak is absent when we calculate the full static structure factor. We characterize the scaling of this peak with parameters characterizing the bottlebrush molecular architecture to aid in the experimental characterization of these molecules by neutron scattering.

## I. INTRODUCTION

Bottlebrush polymers have attracted considerable attention in the last few years due to their unique molecular structural features, and these materials have inspired the design of novel applications as rheological property modifiers,<sup>1</sup> pressure sensors,<sup>2</sup> photonic bandgap materials,<sup>3-5</sup> pH-sensitive probes,<sup>6</sup> supersoft elastomers,<sup>7,8</sup> nanostructured morphologies,<sup>9-13</sup> and drug delivery agents.<sup>14</sup> Despite advances in polymer synthesis techniques for creating branched molecules with precise control of molecular architecture,<sup>15-19</sup> as well as, experimental<sup>7,12,19-27</sup> and simulation,<sup>11,13,28-30</sup> methods to establish structure property relationships between the bottlebrush polymer architecture, a general understanding of the physical properties of these materials remains largely unexplored. Part of the scientific challenge here is that direct experimental measurements of conformational properties in the melt state are difficult and experimental observations of these properties are often performed in solution rather than in the melt state. Moreover, the majority of computational investigations of bottlebrush polymers have been confined to relatively high temperatures in comparison with temperatures relevant for processing and applications. We find this to be a problem because the screen-

ing of excluded volume interactions is rather different in branched polymer melts.

The present paper focuses on bottlebrush polymer melts, which are moderately, but, regularly branched, polymers. We may expect these polymers to be more or less similar in geometry to either linear or randomly branched polymers, depending on the choice of branching parameters defining the bottlebrush architecture. The present work also restricts attention to polymer melts and explores how changes in molecular topology (including also rings and stars in the comparison) influence the chain geometry and melt properties. We observe that configurational properties of bottlebrush polymers in the melt state and the thermodynamic properties of the melt materials strongly resemble unknotted ring polymer melts, over a wide range of model parameters. These materials also resemble star polymer melts for which the number of arms and arm length is moderate, supporting observations by us in an earlier study.<sup>31</sup> Here we emphasize that all these topologically constrained polymers have geometrical conformational characteristics similar to randomly branched polymers ('lattice animals') in the melt state. Our focus here is to obtain a broader understanding of properties for all bottlebrush polymers and the other molecular architectures in order to gain a deeper understanding of their similarities and differences. We emphasize three distinct aspects of bottlebrush melts, namely thermodynamics, conformational properties, and scattering properties. In particular, three basic thermodynamic properties are calculated: segmental density, isobaric thermal expansion

---

<sup>a)</sup>Electronic mail: [alexandros.chremos@nist.gov](mailto:alexandros.chremos@nist.gov)

<sup>b)</sup>Electronic mail: [jack.douglas@nist.gov](mailto:jack.douglas@nist.gov)

sion coefficient, and isothermal compressibility; these thermodynamic properties are crucial for designing materials suitable for 3-D printing and polymer processing. To characterize the conformational properties, we calculate the radius of gyration and its eigenvalues, and the hydrodynamic radius. Finally, we calculate the static structure factor to obtain insights on the packing of the molecules.

Our paper is organized as follows. In Section II we briefly summarize the effect of molecular topology on the conformational properties of polymers in solution and in the melt. Section III contains details of the model and simulation methods. Results of the conformational, thermodynamic, structure, and dynamic properties of bottlebrush melts are presented in Section IV. Section V concludes the paper.

## II. BACKGROUND ON UNIVERSALITY CLASSES OF POLYMERS IN RELATION TO POLYMER TOPOLOGY

Before describing our results, we briefly review known results regarding how the molecular topology influences the conformational properties of flexible polymers in solution and in the melt state to provide a reference point for the classification of bottlebrush polymers.

Polymer topology can have a significant influence on the geometrical characteristics of polymers in solution and in the melt state. Linear and random branched polymers at equilibrium form the most basic classes of polymers, which exhibit universal scaling of their average size in solution (e.g., radius of gyration  $R_g$ ) with increasing molecular mass  $M_w$ . In particular,  $R_g$  scales as  $M_w^\nu$  with  $\nu \approx 10/17 \approx 0.588$  and  $\nu = 1/2$  for self-avoiding walks and lattice animals in three dimensions, respectively.<sup>32–35</sup> Moreover, linear chains and randomly branched polymers also exhibit ‘universality’ in their average shape, which deviates rather significantly from a spherically symmetric mass distribution and from each other. The mass scaling of these polymers is also universal near the  $\theta$ -point in solution at which attractive interactions between the polymer segments compensate the repulsive binary excluded volume interactions. Specifically,  $\nu = 1/2$  for linear chains<sup>36</sup> and  $\nu \approx 2/5$  for randomly branched polymers at their  $\theta$ -point in three dimensions,<sup>37</sup> where binary excluded volume interactions are compensated by attractive polymer-polymer self-interactions.<sup>38,39</sup>

It is also well known that increasing the concentration of swollen linear chain polymers in solution leads to a progressive ‘screening’<sup>40–42</sup> of the repulsive interactions leading to a change of  $\nu$  from dilute solution value  $\nu \approx 10/17$  to  $\theta$ -solvent value  $1/2$ , the mass scaling of an ideal random walk without excluded volume interactions. Randomly branched polymers in their melt state likewise exhibit a reduction in their mass scaling exponent  $\nu$  due to the excluded volume screening. Recent simulation studies have suggested that  $\nu$  for randomly branched polymers in their melt state is exactly

$1/3$ ,<sup>43–46</sup> indicating that these polymers form rather ‘compact’ structures in the melt state, rather than being like randomly branched polymers at their  $\theta$ -point. Screening evidently operates differently between linear chains and randomly branched polymers. Ring polymers in the melt have been shown to exhibit this same type of scaling,<sup>47</sup> strongly suggesting that these polymers belong to the randomly branched polymer universality class when they are in the melt state. Upon dilution, however, ring polymers exhibit the scaling properties of linear chains.<sup>48,49</sup> We note that the compact structure of randomly branched polymers in the melt state arises even when the polymer chains have no loops, i.e., the polymers having tree-like structure, so that loop formation is *not required* for polymers to exhibit the scaling properties of a branched polymer. This feature of branched polymers universal scaling in the melt is relevant to our discussion below of star and bottlebrush polymers, which have no polymer loops.

Percolation clusters are equilibrium randomly branched polymers having an intermediate concentration between isolated swollen branched polymers<sup>39</sup> and a polymer melt state. The mass scaling exponent  $\nu$  for these polymers is consistent with a Flory type estimate of  $\nu$  for branched polymers at their  $\theta$ -point,<sup>39</sup>  $\nu_\theta \approx 2/(d+2)$  for  $d$  less than or equal 6, or in three dimension  $\nu_\theta \approx 2/5$ .<sup>50</sup> We see from Fig. 1 that this relation holds rather well from  $d = 2$  up to 6 dimensions, the upper critical dimension of percolation clusters beyond which mean field theory applies.

We may then expect the value of  $\nu$  for randomly branched polymers in 3 dimensions to show a continuous crossover from  $\nu = 1/2$  to  $1/3$  with increasing polymer concentration, analogous to the crossover of linear polymers from the swollen chain value  $\nu = 3/4$  to a collapsed chain value  $\nu = 1/2$  in their melt state in two dimensions; a scaling with the  $\theta$  point estimate  $\nu = 4/7$  has been reported intermediate concentrations or at moderate molecular mass in the melt.<sup>41</sup> However, it appears that the  $\theta$ -point scaling corresponds to an unstable fixed point due to relevant many-body excluded volume interactions beyond second order.<sup>51</sup> This situation holds both for linear chain polymers in two dimensions and for randomly branched polymers in three dimensions, and, frankly, there is uncertainty whether any true universality exists in the mass scaling in these systems in the melt state.

A basic feature of randomly branched polymers (‘lattice animals’) is that the number of branching points tends to grow linearly with the polymer mass so that such polymers can be thought of as imperfect sheet-like polymers, i.e., having a topological dimensionality of two.<sup>39</sup> This relationship is quantitative and explains the critical dimension and mass scaling exponents of branched polymers noted above.<sup>39</sup> Polymers having different topologies than linear chains and randomly branched polymers raise the question of how their scaling characteristics relate to polymers having a different topological structure. Isolated swollen ring polymers

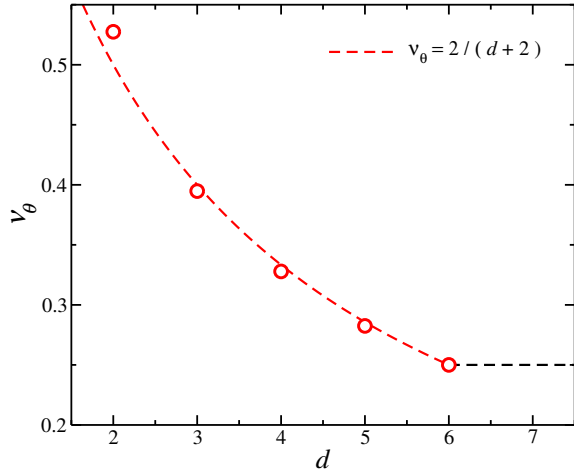


FIG. 1. Mass scaling exponent  $\nu_\theta$  of percolation clusters. The open symbols correspond to numerical estimates of  $\nu$  for percolation clusters taken from the literature.<sup>33,52–58</sup> The dashed line is the Flory-theory prediction for dimensional variation of the mass scaling exponent  $\nu$  for branched polymers with screened binary excluded volume interactions, i.e., percolation clusters.<sup>39</sup>

and star polymers in solution having a fixed number of arms exhibit a mass scaling of isolated swollen linear chains (i.e., self-avoiding random walks) when the arms are long and self-repelling, but recent work has indicated the scaling properties of (unknotted) rings polymers in the *melt state* closely resemble randomly branched equilibrium polymers<sup>40–42</sup> so that these polymers appear to *switch* their universality class with increasing concentration. Simulation of unknotted ring melts and stars having a moderate number of arms<sup>31</sup> ( $f = 5$  to 6 arms) and modest chain lengths also indicate an apparent mass scaling consistent with randomly branched polymers at their  $\theta$ -point condition, i.e.,  $\nu \approx 2/5$ .<sup>37,39</sup> Measurements of randomly cross-linked polymers in solution at relatively high polymer concentrations near their percolation threshold also indicate a value of  $\nu$  near the expected  $\theta$ -point value  $\nu = 0.4$ ,<sup>59</sup> but a mass-scaling exponent consistent with the swollen branched polymer value  $\nu = 1/2$  is obtained when randomly branched polymers are diluted and swollen in a good solvent.<sup>38</sup> This may well be a cross-over effect as in polymers in two-dimensional melts, but this effective scaling behavior seems to be relevant to real ring and star polymers having finite mass.

The geometrical properties of randomly branched macromolecules in the melt state just described have important implications for the chain entanglement. The entanglement molecular mass  $M_e$  of polymer melts has been shown to correlate strongly with the packing length  $p$ , which is defined as the ratio of the chain molecular volume over the square of the chain radius of gyration,  $M_e \sim p^3$ .<sup>60</sup> The fact that the radius of gyration for randomly branched polymers in the melt scales with

polymer mass to a power less than  $1/2$  means that  $p$  must approach infinity in the large mass limit. This would seem to imply that randomly branched polymers should not be “entangled” in the sense of linear chain polymer melts. Given that ring polymers follow the same mass scaling relationship in melt as randomly branched polymers, the present work suggests that bottlebrush polymer melts should also not be entangled, even when the bottlebrush polymers have long chain backbones. Some preliminary observations support this conclusion.<sup>25,61</sup> Of course, randomly branched, ring, and bottlebrush polymers are “ultrasoft” particles that can exhibit molecular clustering and could develop a collective mechanical response in bulk materials by a different “entanglement” mechanism than linear chains.<sup>62–65</sup>

### III. MODEL AND METHODOLOGY

Our system consists of  $N_p$  polymers. A bottlebrush polymer has two main features, namely a linear chain backbone and side chains. The backbone is composed of  $N_b$  segments and the side chains each composed of  $M$  segments. Each bottlebrush polymer has  $f$  side chains, where one of their free ends is grafted along the backbone chain in a uniform fashion. Thus, the total number of interaction centers per bottlebrush polymer is  $M_w = fM + N_b$ . The main focus of the current study is on the following set of molecular parameters: arm lengths having  $M = 2, 5, 10,$  and  $20$  segments, backbone lengths having  $N_b = 5, 10, 20,$  and  $40$  segments, and grafting density  $f/N_b = 1$ . This particular set of parameters leads to a wide distribution of molecular masses ranging from  $M_w = 15$  to  $840$ . We also explore the effects of grafting density  $f/N_b = 1/2$  and  $2$  for bottlebrushes having  $M = 10$ . A schematic that illustrates the bottlebrush molecular architecture and typical molecular conformations for different bottlebrush polymers is presented in Figs. 2a and b.

The interactions between all types of segments are described by the cut-and-shifted Lennard-Jones (LJ) potential where  $\varepsilon$  and  $\sigma$  define the units of energy and length, and a cutoff distance  $r_c = 2.5\sigma$ . The segments along a chain are connected with their neighbors via a stiff harmonic spring,  $V_H(r) = k(r - l_0)^2$ , where  $l_0 = 0.99\sigma$  is the equilibrium length of the spring, and  $k = 2500\varepsilon/\sigma^2$  is the spring constant. In terms of the units of real polymer chains, the beads should be identified with statistical segments of flexible polymer having a typical scale of  $1\text{ nm}$  to  $2\text{ nm}$ .

In our study, we make frequent comparisons to other molecular architectures (linear chains, regular stars, and unknotted rings) that have been studied previously by the authors with the same model. We briefly describe the modeling for these architectures here from the perspective of bottlebrush model utilized in the current study. A star polymer is effectively a bottlebrush having the shortest possible backbone, i.e.,  $N_b = 1$ . Thus,

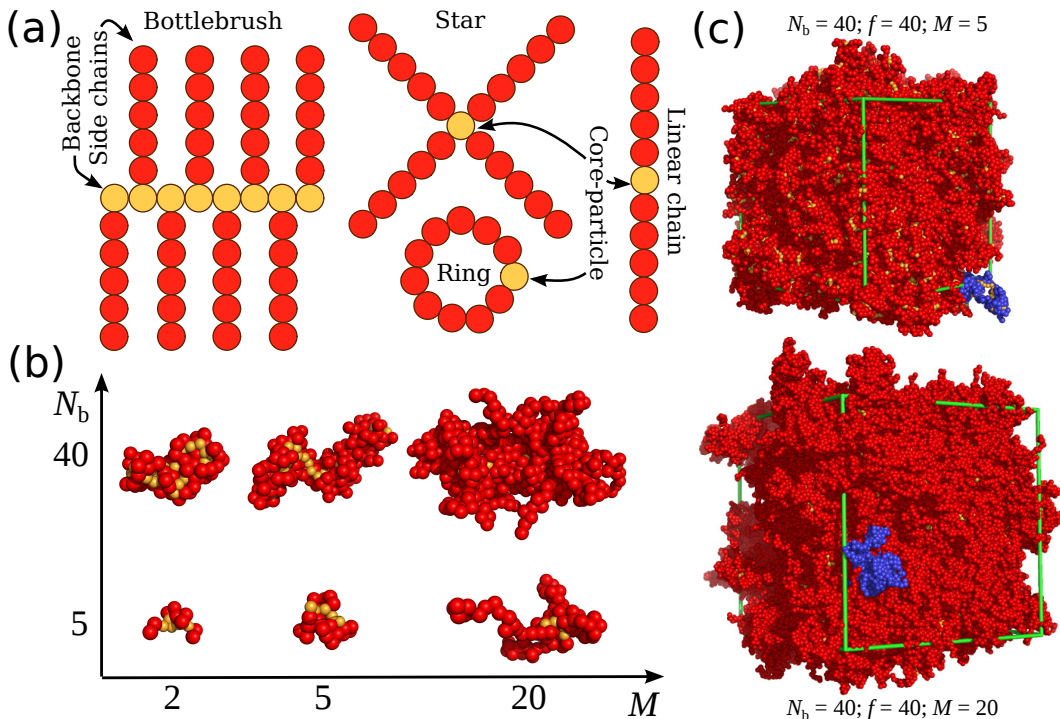


FIG. 2. (a) Schematic illustration of the topological architecture of bottlebrushes, regular stars, linear chains, and unknotted rings. (b) Typical molecular conformations of bottlebrush polymers with variation of the backbone length  $N_b$  and side chain length  $M$ . The side chain segments are represented with red color and the backbone segments are represented with orange color. (c) Typical snapshots of two different types of bottlebrush polymer melt. A single bottlebrush polymer is picked from the melt and its side chain segments depicted with blue color.

the backbone becomes the core particle at which  $f$ -chains are grafted on its surface. A linear chain is a special case of star polymers and by extension of bottlebrushes, from the bottlebrush model one recovers the linear chain molecular architecture by having  $N_b = 1$  (as in star polymers) and  $f = 2$ . Ring polymers are linear chains having their free ends bonded with each other, this molecular architecture is special since it cannot be recovered from the bottlebrush model through the variation of molecular parameters. A schematic that illustrates all the different molecular architectures is presented in Fig. 2a.

Simulations were performed in a cubic box with length  $L$ ; periodic boundary conditions were applied in all three directions. We utilized the large-scale atomic/molecular massively parallel simulator (LAMMPS).<sup>66</sup> Simulations were performed in the  $NVT$  ensemble after equilibration in the  $NPT$  ensemble at the desired temperature. Time averaging was conducted for  $O(10^8)$  time steps after equilibration. The time step was set to  $\delta t = 0.005 \tau$ , where  $\tau = \sigma(m_b/\varepsilon)^{1/2}$  is the unit of time. Temperature and pressure are measured in units of  $\varepsilon/k_B$  and  $\sigma^3/\varepsilon$ , respectively. Simulations were performed at different temperatures  $T = 0.5, 0.6, 0.7$ , and  $0.8$ , and  $\langle P \rangle \approx 0.1$  in reduced units. We note that the initial configurations for obtaining equilibrated bottlebrush polymer melts at desired temper-

ature and pressures were generated from equilibrated systems at higher  $T$ . For example, to obtain an equilibrated polymer system at  $T = 0.7$ , an equilibrated system at  $T = 0.8$  was used. This sequential equilibration allowed us to reach lower temperatures without the bottlebrush polymers getting trapped in meta-stable states. We determine whether a polymer system is equilibrated when the system's potential energy and conformational properties of the bottlebrush polymers do not change over an extended time period  $O(10^7)$ . An additional internal consistency check was performed through comparison of the structure with the isothermal compressibility, for more details see Subsection IV E.

#### IV. RESULTS & DISCUSSION

We first obtain the average segmental density of bottlebrush polymer melts for different molecular parameters as well as its dependence with  $T$ . Following this analysis, we determine the average polymer size of bottlebrush polymers having different molecular parameters as a function of molecular mass. This provides a relevant characteristic length scale necessary to understand how different molecular features contribute to the mass scaling of polymer size. Subsequently, we use these length scales to quantify the average molecular shape of

bottlebrushes. Afterwards, we calculate the static structure factor for the backbone segments of these systems and in particular probe the variation of the location of the primary peak as a function of different molecular parameters. Finally, we briefly study the dynamical behavior of bottlebrush polymers. In all subsections, we make comparisons to other molecular architectures, namely linear chain, star, and ring.

### A. Basic thermodynamic properties of bottlebrush melts

The segmental density ( $\rho_b = N_p M_w / V$ ) quantifies the packing efficiency of polymers in the melt state and it is a useful quantity in probing the differences in packing between different polymer topologies. Within the bottlebrush parameter space explored in our study, we find that all bottlebrush polymer melts have nearly the same value of  $\rho_b$ , irrespective of the molecular mass, grafting density, and side chain length; see Fig. 2. This means that bottlebrush polymers do not follow the typical behavior of linear chains, which exhibit significant  $M_w$  dependence. A comparison between linear chains, corresponding to the case of  $f = 2$ , and bottlebrush polymers is presented in Fig. 3, where it is evident that even at a relative large molecular mass  $M_w \approx 100$  the differences in  $\rho_b$  between bottlebrush polymers and linear chains are noticeable; as a point of reference, we note that the molecular mass of linear chains based on the bead-spring model for which entanglements are reported to occur  $M_{w,e} \approx 85$ .<sup>67</sup> Moreover, all bottlebrush polymers explored in our current study exhibit trends in  $\rho_b$  that are quantitatively similar to both unknotted ring polymer melts and star polymers having  $f = 5$  to 6 arms. Indeed, as we discussed at the introduction, ring polymer melts exhibit no or little  $M_w$  dependence.<sup>68</sup> We also find that all the bottlebrush polymers explored here exhibit the same  $M_w$  dependence behavior as the unknotted rings, but also we find  $\rho_b(\text{bottlebrush}) \approx \rho_b(\text{rings})$ . This relation is striking because it means that the molecular topology, whether one thinks about in terms of number of free ends and/or segmental connectivity, is not the primary factor influencing  $\rho_b$  of polymer melts.

To better understand these observed  $\rho_b$  trends, we explore the changes in volume with variation of  $T$  and  $P$ . In particular, we calculate the isobaric thermal expansion coefficient  $\alpha_P$  which describes the fractional change in volume per degree change in  $T$  at constant  $P$ ,

$$\alpha_P = \frac{1}{V} \left( \frac{\partial V}{\partial T} \right)_P, \quad (1)$$

and isothermal compressibility  $\kappa_T$  which describes the fractional change in volume per degree change in  $P$  at constant  $T$ ,

$$\kappa_T = -\frac{1}{V} \left( \frac{\partial V}{\partial P} \right)_T. \quad (2)$$

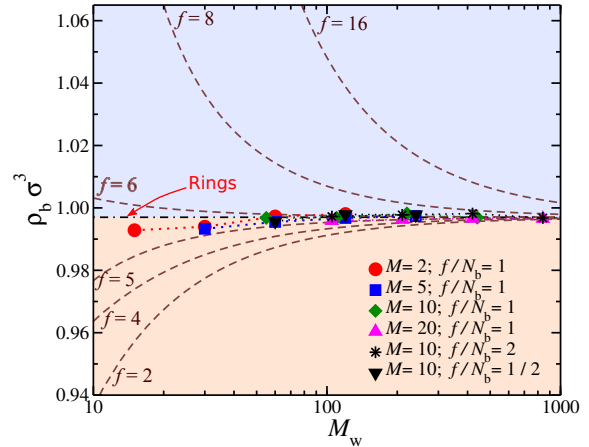


FIG. 3. Segmental density  $\rho_b$  at temperature  $T = 0.5$  and fixed pressure as function of the molecular mass,  $M_w$ . Symbols correspond to bottlebrush polymer melts. Dashed lines correspond to segmental correlations based on the Eqn. 4 for star polymers (equivalent to bottlebrushes having a backbone length  $N_b = 1$ ) and the dot-dashed line represents the segmental density of ring polymers. For more information on the results for star and ring polymers; see Refs. 69 and 31. The highlighted regions correspond to polymers having (bottom) highly anisotropic linear chain-like conformations and (top) highly symmetric particle-like conformations.

A series of simulations were performed at different pressures ( $P = 0, 0.05, 0.10, 0.15, 0.20$ , and  $0.25$ ) and temperatures ( $T = 0.55, 0.60, 0.65, 0.70$ , and  $0.75$ ) and the average volume was obtained. Based on the  $PVT$  behavior we fit in two step process the volume as a function of  $P$  and  $T$ ,

$$V(T, P) = -\frac{1}{2}k_2TP^2 - P(k_1T + k_3) + k_4T + k_5, \quad (3)$$

where  $k_1, k_2, k_3, k_4$ , and  $k_5$  are fitting parameters. While these fitting parameters are system size dependent, the properties of interested to us, i.e.,  $\alpha_P$  and  $\kappa_T$ , are not system size dependent in the  $T$  range of our investigation. In the first step, we fit the  $PVT$  data to Eq. 3 at  $P = 0$  and thus obtaining the  $k_4$  and  $k_5$  coefficients; note that  $k_4$  is  $\alpha_P V$  at  $P = 0$ . In the second step, we fit the  $PVT$  data to obtain the rest of the fitting parameters namely  $k_1, k_2$ , and  $k_3$ . Once we have all the parameters, we obtain  $\alpha_P$  and  $\kappa_T$  through differentiation of Eq. 3 at the desired thermodynamic conditions within the boundaries of the fitting mentioned above. The parameters of Eq. 3 for each molecular architecture and molecular mass is presented in Table I.

The resulting  $\alpha_P$  and  $\kappa_T$  for bottlebrushes, linear chains, stars, and rings are presented in Fig. 4. Momentarily we focus on stars and linear chains. Highly branched star polymer melts have higher values of  $\rho_b$  and at the same time the fractional change in volume per degree in  $T$  or  $P$  is smaller than linear chain melts. We offer the following interpretation in terms of entropy,  $S$ . We add that  $\alpha_P$  can be easily ex-

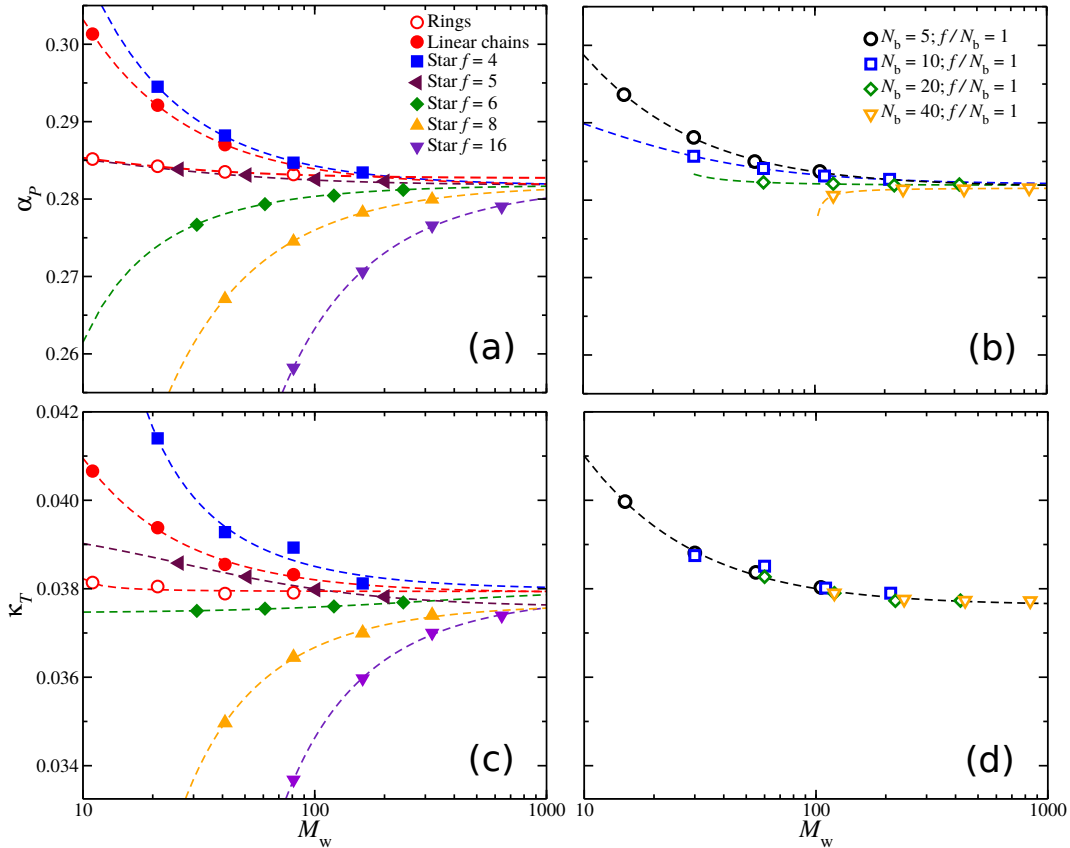


FIG. 4. (a-b) Isobaric thermal expansion coefficient,  $\alpha_P$ , and (c-d) isothermal compressibility,  $\kappa_T$ , as a function of molecular mass,  $M_w$ , at temperature  $T = 0.65$ . Results for various molecular architectures are presented: (a & c) linear chains, stars, and ring polymers; (b & d) bottlebrush polymers. Results for different molecular architectures are also presented. The dashed lines are fits based on Eqn. 4.

pressed in terms of entropy via the Maxwell relations as  $\alpha_P = -(\partial S/\partial P)_T/V$ .<sup>70</sup> Highly branched star polymers have significantly smaller number of possible configurations than their linear chain analogues. In other words, highly branched stars have smaller conformational entropy than linear chains. Decreasing  $T$  or increasing  $P$  in highly branched star melts causes smaller changes in volume for the same variation in  $T$  or  $P$  with respect to linear chains. This means that rate of change in entropy is smaller between highly branched stars and linear chains, meaning that even though the highly branched stars have lower conformational entropy than linear chains, the stars lose their entropy, as thermodynamic conditions change, slower than linear chains. This line of thinking is not always true. Specifically, star polymers having  $f = 4$  arms, not only have segmental density higher than the linear chains (see Fig. 2), but also they exhibit higher fractional change of volume with variation of  $T$  and  $P$  than their linear chain analogues. A possible interpretation about this behavior is that stars having  $f = 4$  arms are ‘soft’ particle-like structure that pack in the melt state more efficiently than linear chains as it is evident from the segmental density trends presented in Fig. 2, but at the same time the molecular

packing is sensitive to the changes in the molecular conformations with  $T$  and  $P$  as it is evident from the  $\alpha_P$  and  $\kappa_T$  trends presented in Fig. 4. These observations reflect a competition between segmental and molecular packing that deserves a deeper appreciation and it will be part of a future study.

Between the two extremes, highly anisotropic linear chains and highly symmetric particle-like molecules, there is a crossover point between these two behaviors. As discussed above for  $\rho_b$ , we find a number of different molecular architectures including bottlebrush, ring, and star polymers having  $f = 5$  to 6 arms to exhibit a behavior near this crossover, see Fig. 4. For example, ring polymers exhibit not only a molecular mass independent  $\rho_b$ , but also  $\kappa_T$  and  $\alpha_P$  have the same behavior. Similar trends are found in  $\rho_b$ ,  $\kappa_T$ , and  $\alpha_P$  for bottlebrush polymers having  $N_b > 5$ . Curiously, ring polymers exhibit similar trends in  $\kappa_T$  with star polymers having  $f = 6$  and similar trends in  $\alpha_P$  with stars having  $f = 5$ . On the other hand, bottlebrush polymers tend to have similar trends in  $\kappa_T$  with star polymers having  $f = 5$  and similar trends in  $\alpha_P$  with stars having  $f = 6$ . Irrespective of minor differences between these molecular architectures, bottlebrush polymers are overall sur-

TABLE I. Fitting parameters  $k_1$ ,  $k_2$ ,  $k_3$ ,  $k_4$ , and  $k_5$  of the volume  $V(T, P)$  as function of temperature and pressure based on Eq. 3 for different molecular architectures (linear chains, stars, rings, and bottlebrushes) and molecular masses  $M_w = fM + N_b$ . We also use the average absolute deviations (AAD%) for evaluating the performance of Eq. 3.

	$N_p$	$N_b$	$f$	$M$	$k_1$	$k_2$	$k_3$	$k_4$	$k_5$	AAD%
Linear chains and stars	400	1	2	5	417.52	-59.04	-78.09	1430.78	3748.38	0.022
	400	1	2	10	724.76	-66.29	-118.52	2630.16	7168.97	0.019
	400	1	2	20	1372.69	-161.12	-218.15	5029.00	14011.20	0.017
	400	1	2	40	2652.21	-110.54	-416.37	9825.72	27680.00	0.015
	400	1	4	5	730.65	-198.20	-107.83	2566.02	6923.08	0.016
	400	1	4	10	1397.90	-285.24	-225.39	4966.98	13762.20	0.015
	400	1	4	20	2694.46	-554.59	-405.74	9749.56	27435.70	0.015
	400	1	4	40	5215.25	-1174.88	-753.89	19364.40	54818.20	0.014
	400	1	5	5	824.32	-132.90	-119.61	3051.60	8621.69	0.014
	400	1	5	10	1617.87	-211.93	-233.15	6056.74	17169.80	0.013
	400	1	5	20	3239.78	-878.37	-455.69	12058.90	34271.60	0.015
	400	1	5	40	6471.52	-1146.20	-962.90	24071.00	68475.10	0.014
	400	1	6	5	917.16	-233.95	-109.96	3533.02	10309.50	0.055
	400	1	6	10	1961.53	-446.92	-303.03	7140.12	20567.10	0.013
	400	1	6	20	3880.40	-788.47	-582.65	14333.40	41097.50	0.015
	400	1	6	40	7730.13	-1742.26	-1125.40	28739.10	82153.60	0.014
	400	1	8	5	1169.34	-274.76	-172.84	4423.80	13464.40	0.012
	400	1	8	10	2390.48	-520.60	-316.44	9218.46	27152.00	0.014
	400	1	8	20	5034.05	-919.04	-751.70	18827.90	54512.90	0.014
	400	1	8	40	9996.51	-2172.12	-1364.89	38004.80	109272.00	0.014
400	1	16	5	1928.99	-529.24	-166.40	8195.50	26046.10	0.008	
400	1	16	10	4317.09	-946.55	-415.72	17797.40	53413.80	0.011	
400	1	16	20	8985.28	-1674.78	-858.28	36999.30	108145.00	0.012	
400	1	16	40	19794.20	-5263.62	-2593.60	75372.90	217641.00	0.014	
Rings	400	1	2	5	369.03	-70.88	-59.52	1337.60	3756.07	0.018
	400	1	2	10	673.73	-130.70	-94.87	2542.66	7174.95	0.017
	400	1	2	20	1331.27	-270.36	-197.41	4951.72	14012.90	0.015
	400	1	2	40	2623.26	-625.83	-378.92	9769.64	27689.50	0.015
Bottlebrushes	3200	5	5	2	4327.90	-1647.17	-686.14	15113.50	40925.50	0.019
	3200	5	5	5	8232.04	-1450.66	-1342.93	29580.80	82006.90	0.016
	3200	5	5	10	14931.40	-3407.46	-2407.85	53510.50	150352.00	0.015
	2400	5	5	20	20822.50	-4753.04	-3187.41	76211.00	215420.00	0.015
	3200	10	10	2	7951.70	-2134.49	-1132.00	29244.30	81988.50	0.019
	1600	10	10	5	7616.98	-3662.61	-838.85	29053.50	82104.90	0.014
	1600	10	10	10	14218.50	-2887.31	-2050.26	53073.20	150457.00	0.019
	1200	10	10	20	20057.50	-4210.41	-2767.57	75843.70	215466.00	0.014
	1600	20	20	2	7799.32	-2037.84	-1092.25	28861.50	82107.80	0.015
	800	20	20	5	7665.31	-887.07	-1117.01	28840.70	82114.70	0.013
	800	20	20	10	13996.90	-1668.35	-2042.43	52812.70	150507.00	0.012
	600	20	20	20	20229.20	-4062.14	-2936.56	75651.30	215491.00	0.014
	800	40	40	2	7691.50	-1570.60	-1091.94	28668.60	82164.60	0.013
	400	40	40	5	7677.79	-1513.66	-1100.76	28746.60	82100.30	0.017
	400	40	40	10	14105.90	-2734.90	-2045.29	52706.90	150518.00	0.014
	300	40	40	20	20191.70	-4165.08	-2909.76	75510.80	215517.00	0.013

prisingly similar to rings and stars having a moderate number of arms in terms of  $\rho_b$ ,  $\kappa_T$ , and  $\alpha_P$ . While similarities between bottlebrush and star polymers are anticipated due to their similarities in their branching topology, which becomes more obvious for small molecular mass bottlebrush polymers, it is not so obvious why bottlebrush polymers exhibit trends that are so similar to unknotted ring polymers. Another consequence of  $\rho_b$ ,  $\kappa_T$ , and  $\alpha_P$  exhibiting little variation with  $M_w$  is that polymers melts having these molecular architec-

tures will have nearly the same segmental density over a wide range of  $T$  and  $P$ .

The trends for all molecular architectures show that as  $M_w$  increases the thermodynamic properties converge to approximately the same point, suggesting that the effects of molecular architecture diminish as  $M_w \rightarrow \infty$ . We note that the point at which they converge depends on the nature of molecular architecture. For example, polymers having  $M_w \rightarrow \infty$  at thermodynamic conditions of  $T = 0.65$  and  $P = 0.1$ ,  $\kappa_T \approx 0.0378$ . While

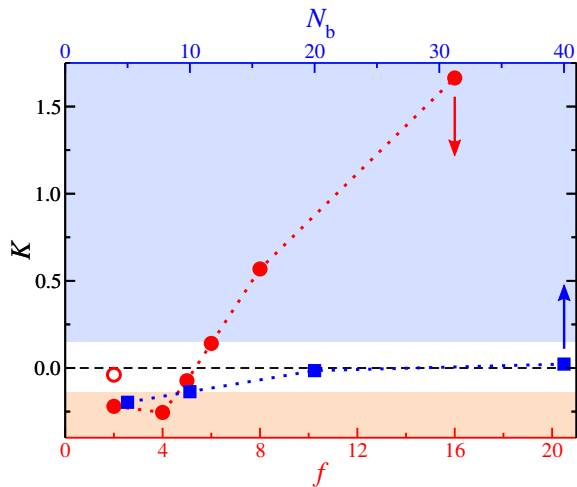


FIG. 5. Parameter  $K$  in Eq. 4 for isobaric thermal expansion  $\alpha_P$  for different molecular architectures. Symbols represent rings (open circle), linear and star polymers (filled circles), and bottlebrush polymers (squares) having grafting density  $f/N_b = 1$  and side chain length  $M = 10$ . The highlighted regions correspond to polymers having (bottom) highly anisotropic linear chain-like conformations, (top) highly symmetric particle-like conformations, and (middle) a regime at which the  $\alpha_P$  trends are relatively insensitive to molecular mass variation.

bottlebrush polymers, rings, and stars having  $f = 6$  arms reach to this thermodynamic point for  $M_w < 100$ , stars having  $f = 16$  require  $M_w > 1000$  to reach approximately to the same point. To organize our findings, we utilize Dobkowski’s correlation function:<sup>71</sup>

$$Q(M) = Q_\infty - \frac{K}{M_w + M_w^*}, \quad (4)$$

where  $Q$  is a structural or dynamical property of interest,  $Q_\infty$  is the value of  $Q$  at infinite molecular mass, and  $K$  and  $M_w^*$  are empirical constants. Properties like the glass transition temperature ( $T_g$ ) and monomer density are shown to have the same functional chain-length dependence,<sup>72</sup> suggesting a close relation between thermodynamic properties and dynamics. Based on our model, we have shown in previous work that Eqn. 4 can describe the segmental density and glass transition temperature of linear chains, star polymers, and ring polymers over a wide range of molecular masses.<sup>31,69</sup> The parameter  $K$  represents the degree of deviation from the  $Q_\infty$  and its sign the direction of this deviation. The general trend that we find for parameter  $K$  is that three regimes can be easily identified irrespective of whether we study  $\rho_b$ ,  $\alpha_P$ , and  $\kappa_T$ . An example based on the fitting of the  $\alpha_P$  values is presented in Fig. 5. In the first regime, we find linear chains and star polymers of  $f < 4$ , which exhibit similar values of  $K$ . In the second regime,  $K \approx 0$  and the molecular architectures that exhibit this trend are ring polymers, stars having  $f = 5$  and 6 arms, and bottlebrush polymers having  $N_b \gtrsim 10$ . The observed trends for  $K$  from the fitting of  $\alpha_P$  and  $\kappa_T$

reinforce our argument that polymers having topologically distinct molecular structures can exhibit similar thermodynamic properties and the glassy dynamics because their overall molecular shape (size, softness, etc.) is the primary factor; molecular topology is important in as much as the polymer topology influences the average molecular shape.

## B. Mass scaling exponent for molecular size

The size of a polymer is an important quantity to determine different material properties and the mass scaling of polymer size can provide insight into the way polymers occupy space and pack with each other. To determine the “average size” of our model bottlebrush polymers in the bulk, we calculate the average radius of gyration,  $\langle R_g \rangle$ , and the average hydrodynamic radius  $\langle R_h \rangle$ ; the calculation of  $\langle R_h \rangle$  is based on the use of path-integration algorithm ZENO, which calculates hydrodynamic, electrical, and shape properties of polymer and particle suspensions.<sup>73–75</sup> The mass scaling of the average polymer size as described by  $R_g$  and  $R_h$  increases with mass as a power-law, i.e.,  $\langle R_g \rangle \propto M_w^\nu$  and  $\langle R_h \rangle \propto M_w^\mu$ , as expected, see Fig. 6a. The exponents in these power-law relations define the ‘fractal dimension’ of the polymers ( $d_f = 1/\nu$ ), e.g., for linear polymer chains in a melt (or in  $\theta$ -solvent),  $\nu = 1/2$ , the well-known value for random coil polymers.<sup>76,77</sup> Increasing the degree of molecular complexity leads to more contracted molecular conformations, meaning that their exponent is smaller than a random walk chain ( $\nu = 1/2$ ), but larger than a fully collapsed polymer in its globular state ( $\nu = 1/3$ ). This scaling is remarkably similar to experimental and simulation studies of ring polymers in the melt state.<sup>47,78</sup>

For bottlebrush polymers, there are different ways to increase the molecular mass. Here, we will examine two ways: the first way is to increase  $N_b$  by keeping the  $f/N_b$  and  $M$  fixed, and the second way is to increase  $M$  by keeping fixed  $f/N_b$  and  $N_b$ . In the first way to increase  $M_w$ , the mass scaling of  $\langle R_g \rangle$  does not appear to fit one power-law relation. For small values of  $N_b$ , bottlebrush polymers (irrespective of  $M$ ) tend to follow a power-law relation  $\langle R_g \rangle \sim M_w^{0.36}$ ; the exponent is close to  $1/3$ , as found before for rings in the melt state.<sup>47</sup> The determination of this scaling exponent requires additional simulations since at those molecular parameters there are large fluctuations in size, making calculations of the average polymer size challenging. As the bottlebrush backbone becomes longer, we observe a change in  $\nu$  from 0.36 to a higher value. Presumably, this higher exponent is  $1/2$  since for long backbones with respect to the side chain length, the bottlebrush then resembles a linear chain which exhibits random walks statistics.

In the second way of increasing bottlebrush polymer  $M_w$ , we find that the results, as seen in Fig. 7, fit well to a power-law relation, i.e.,  $\langle R_g \rangle \sim M_w^\nu$ , suggesting that the second way is more natural to probe the mass

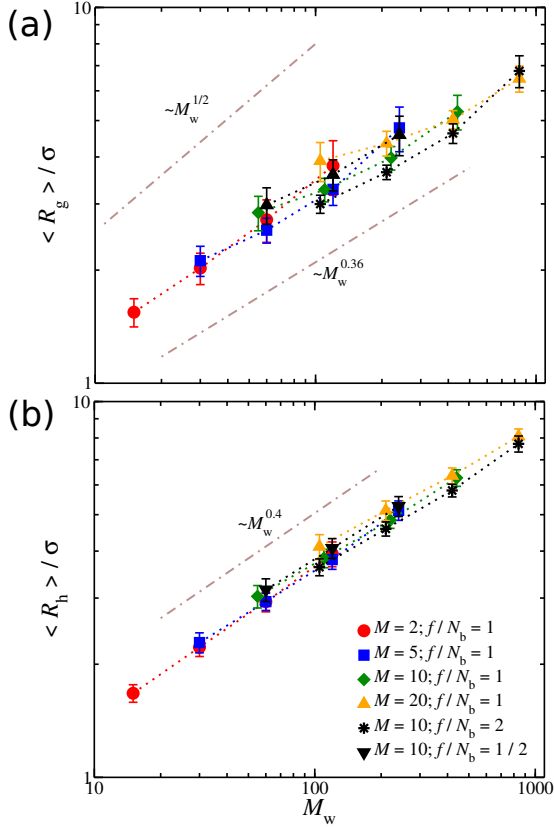


FIG. 6. (a) Average radius of gyration,  $\langle R_g \rangle$ , of bottlebrush polymers and (b) average hydrodynamic radius,  $\langle R_h \rangle$ , as a function of the molecular mass  $M_w$  at temperature  $T = 0.5$ . The errorbars represent two standard deviations. The dot-dashed lines correspond to a power-law relation as a guide for the eye.

scaling exponent in bottlebrush polymers. However,  $\nu$  changes from nearly  $1/2$  for  $N_b = 5$  to approximately  $1/4$  for  $N_b = 40$ , see inset of Fig. 7. The exponent  $\nu \approx 1/4$  occurs for lattice animals in the complete absence of excluded volume interactions, which is an exact asymptotic result above  $d = 8$  dimensions but only a transient exponent in  $d = 3$ . This exponent cannot be stable with increasing polymer mass, however, and ultimately  $\nu \gtrsim 1/3$  if the polymers are space filling. This general trend holds for all temperatures explored in our study. A similar mass scaling crossover is physically observed in the radius of gyration of dendrimer molecules having a high generation number where excluded volume interactions inhibit further cluster growth.<sup>79</sup> The interpretation of this mass scaling exponent is closely related to the internal density distribution. Specifically, low generation dendrimers have a higher density in the core that gradually decreases towards the periphery giving rise to a fractal-like structure, while high generation dendrimers tend to have a homogeneous spherical density distribution.<sup>79</sup> We anticipate a similar trend for bottlebrush polymers as well. As  $M$  increases for bot-

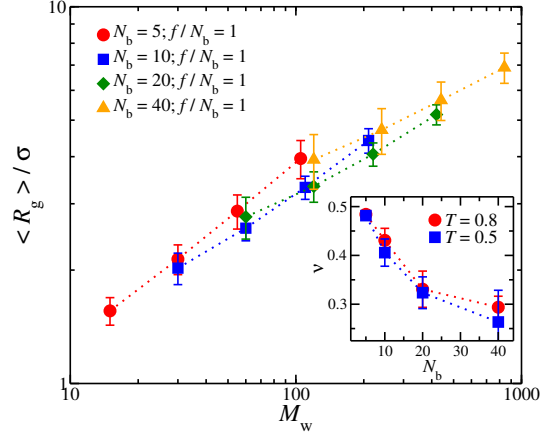


FIG. 7. Average radius of gyration,  $\langle R_g \rangle$ , of bottlebrush polymers having grafting density  $f/N_b = 1$  as a function of the molecular mass  $M_w$  at temperature  $T = 0.8$ . The errorbars represent two standard deviations. Inset: Mass scaling exponent  $\nu$ , determined from  $\langle R_g \rangle \sim M_w^\nu$  at fixed backbone chain lengths and with variation of side chain length  $M$ . Results for different temperatures ( $T = 0.5$  and  $0.8$ ) are also presented. The errorbars represent one standard error.

tlebrush polymers having short backbones, the overall size of the polymer varies in the range  $2/5 \lesssim \nu \lesssim 1/2$ . This similarity of bottlebrush polymers to stars is not surprising given the similarities in their density distributions, which are characterized by a dense core and a density that gradually away decreases from the polymer center of mass.

This geometrical relationship also means that the corona of bottlebrush polymers should be relatively ‘soft’, thus allowing greater interpenetration of neighboring polymers. However, for bottlebrush polymers having longer backbones, an increase of the side chain length leads to a reduction of the interpenetration from neighboring molecules and an overall reduction of the number of segmental heterocontacts. This is accompanied by the bottlebrush polymer adopting a more compact molecular configuration around the backbone, thus raising similarities also with high generation dendrimers.<sup>79–82</sup>

While the determination of the bottlebrush size with  $\langle R_g \rangle$  results in different outcomes with variation of molecular parameters, the  $\langle R_h \rangle$  results display remarkable similarity for all molecular parameters explored in our study. In particular, we find a mass scaling  $\langle R_h \rangle \sim M_w^\mu$  for all bottlebrush polymers, where  $\mu = 2/5$ . Similar mass scaling exponents for  $R_h$  has been found for ring polymers and stars having  $f = 6$  arms.<sup>83</sup> For comparison we note that linear chains exhibit a mass scaling for  $R_h$  with  $\mu \approx 0.5$ , while star polymers exhibit a range of mass scaling exponents in the range of  $0.42 < \mu < 0.5$  and the lowest  $\mu$  value is found for stars having  $f \approx 6$  arms; see Ref. 83. Moreover, we found<sup>83</sup> a nearly universal power-law relation between self-diffusion and  $R_h$ ,

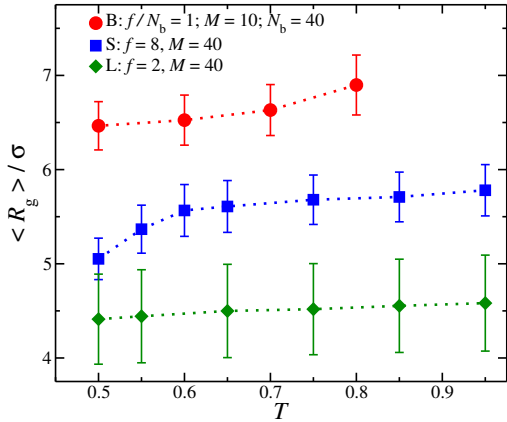


FIG. 8. Radius of gyration as a function of temperature,  $T$ , for different molecular architectures. The notation B, S, and L correspond to bottlebrush, star, and linear chain polymers, respectively. The errorbars represent one standard deviation.

meaning that the molecular size and shape are of primary importance for diffusion in polymer melts. In the case of bottlebrush polymers, this means that the shape of the polymers changes so that the diffusion scales with the molecular mass, irrespective of the molecular structure. The origin of this near universal scaling is currently unclear to us.

We next briefly focus on the effect of  $T$  on the polymer size among different molecular architectures. It is often assumed that the conformational properties of linear polymer chains in a melt are essentially the same as those for “unperturbed” chains without excluded volume interactions, first suggested by Flory.<sup>32</sup> This behavior was theoretically explained by Freed and Edwards<sup>84</sup> as arising from the “screening” of excluded volume interactions with increasing polymer concentration. We find that linear chains exhibit a small degree of swelling over the  $T$  range that we explore in our study (Fig. 8) and we find good agreement with the scaling predicted by Freed and Edwards in the case of linear polymer chains. For star polymers, however, we find that they exhibit an appreciable variation, indicating that screening of the excluded volume interactions operate differently in branched macromolecules in the melt. Specifically,  $\langle R_g \rangle$  dependence with  $T$  is similar with that of linear chains for  $T > 0.6$ , but  $\langle R_g \rangle$  decreases at a higher rate as  $T$  decreases for  $T < 0.6$ , meaning that the stars exhibit a non-trivial shrinking behavior in the melt that is not anticipated from our understanding from linear chains. Bottlebrush polymers also exhibit a deviation from linear chains, meaning that the rate of change of  $R_g$  with  $T$  is not constant. These observations reinforce the argument that the “Flory theorem,” indicating that polymer chains in the melt are similar to ideal chains without excluded volume, does not generally extend to polymers having a non-linear topology.<sup>31</sup>

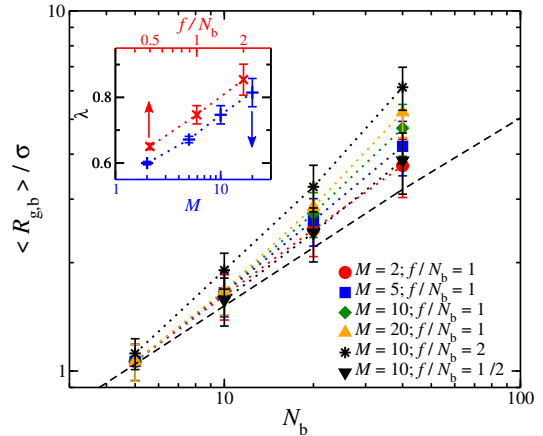


FIG. 9. Radius of gyration of the backbone chain of bottlebrush polymers,  $R_{g,b}$ , as a function of the backbone length,  $N_b$  at temperature  $T = 0.8$ . The errorbars represent two standard deviations. The dashed line corresponds to linear chains in melt. Inset: Mass scaling exponent  $\lambda$  as determined from the relation,  $R_{g,b} \sim N_b^\lambda$ . The errorbars represent one standard error.

### C. Backbone conformation characterization

In the previous subsection, we calculated the size of the whole bottlebrush molecule. We first calculate the radius of gyration of the backbones,  $R_{g,b}$ , to determine the influence of side chains on the conformational properties of the backbone chains. The resulting  $R_{g,b}$  for bottlebrush polymers is presented in Fig. 15. It is evident that an increase in  $f/N_b$  or in  $M$  leads to an increase in  $R_{g,b}$ . We quantify this effect by fitting the  $R_{g,b}$  values to a power-law relation  $R_{g,b} \sim N_b^\lambda$ . This exponent is found to be greater than  $\lambda > 1/2$  for backbone chains, meaning that the mass scaling exponent  $\lambda$  is intermediate between from the coil exponent of linear chains in the melt and extended chain conformation of a polymer in a high grafting density brush layer. In particular, the effective exponent  $\lambda$  ranges for the molecular parameters that we explore from 0.6 to 0.85, as illustrated at the inset of Fig. 9. Several previous studies of bottlebrush polymers in solution have shown that the side chains alter the conformational properties of the backbone.<sup>28,29,85,86</sup> Evidently, the swelling in solution is larger than found under melt conditions. Recent simulations have also shown that there are significant in the concentration-dependent changes in the size of the bottlebrush polymers in solution.<sup>87</sup> Recent experiments by Bates et al.<sup>88</sup> have also indicated that the conformation of the bottlebrush backbones is more ‘coiled’ than initially anticipated, which is consistent with our findings.

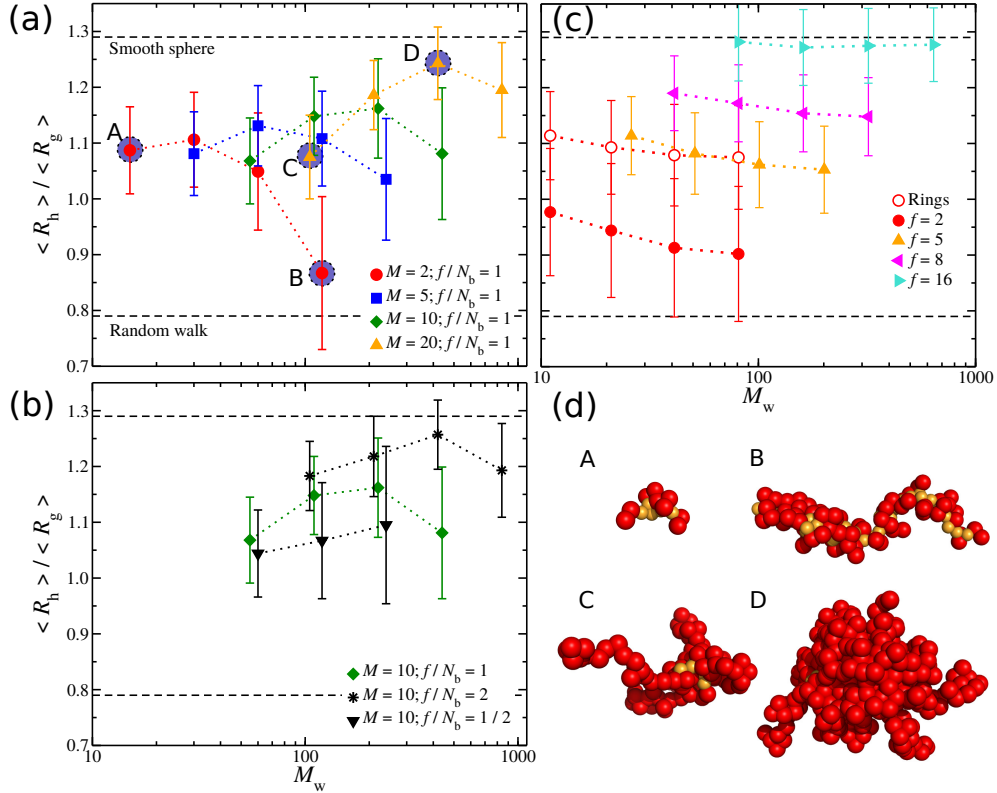


FIG. 10. Ratio of the average hydrodynamic radius over the average radius of gyration,  $\langle R_h \rangle / \langle R_g \rangle$  of bottlebrush polymers having (a) grafting density  $f/N_b = 1$  and (b) side chain length  $M = 10$  at different grafting densities, as a function of the molecular mass,  $M_w$ . (c) Typical examples of  $\langle R_h \rangle / \langle R_g \rangle$  trends for stars and rings based on findings from a previous study.<sup>83</sup> The errorbars represent two standard deviations and the dashed lines correspond to the values of a smooth sphere  $\langle R_h \rangle / \langle R_g \rangle = 1.29$  and random walks  $\langle R_h \rangle / \langle R_g \rangle = 0.79$ . (d) Screenshots of typical molecular configurations of bottlebrush polymers with molecular parameters as indicated in (a).

#### D. Average molecular shape of bottlebrush polymers

Now that we have characterized the mass scaling of the molecular size of bottlebrush polymers with molecular parameters, we focus on the average molecular shape of these model branched polymers. Linear chain polymers exhibit highly anisotropic conformations,<sup>89,90</sup> while other molecular architectures, such as star<sup>83,91–95</sup> and rings<sup>47,83,91,92,96,97</sup> polymers, tend to exhibit less anisotropic conformations. Here we use two different approaches to quantify shape.

In the first approach, we utilize the difference in variation between  $R_h$  and  $R_g$  to quantify the shape of the molecular conformations. Indeed, the ratio  $R_h/R_g$  is often used as a descriptor to quantify the shape of polymers.<sup>73,74</sup> The values of  $R_h/R_g$  for a smooth sphere is 1.29, for a random walk is 0.79, and for an infinite long rod is 0.<sup>98,99</sup> Each molecular architecture (linear chain, ring, and star) exhibits a relatively simple trend as  $M_w$  increased, as discussed in our previous study.<sup>83</sup> For example,  $\langle R_h \rangle / \langle R_g \rangle$  of linear chains decreases from the smooth sphere limit (when  $M_w = 1$ ) to the more anisotropic conformations characteristic

of polymer random coils  $\langle R_h \rangle / \langle R_g \rangle \approx 0.79$ . Highly branched stars exhibit little variation with  $M_w$  and the value of  $\langle R_h \rangle / \langle R_g \rangle$  is close to the value of a smooth sphere  $\langle R_h \rangle / \langle R_g \rangle \approx 1.29$ . Bottlebrush polymers exhibit a complex behavior, as illustrated in Fig. 10a and b, that we are going to decipher it here. For short backbones, the bottlebrush polymers have  $\langle R_h \rangle / \langle R_g \rangle$  values intermediate between the random walk and smooth sphere limits. Curiously, as  $N_b$  increases then the shape of the bottlebrush is more spherically symmetric. This effect becomes more pronounced for bottlebrushes having side chains of length comparable with the length of the backbone chain and around this point we observe a maximum in  $\langle R_h \rangle / \langle R_g \rangle$  as function of  $M_w$ , see Fig. 10a. Once the backbone chain length becomes significantly larger than the side chain length, then the overall shape of the bottlebrush polymer becomes more anisotropic. Increasing the grafting density along the bottlebrush backbone makes bottlebrush shape more spherical shape, see Fig. 10b.

To better understand the average shape of bottlebrush polymers, we utilize a different approach in quantifying the shape of these molecules. In the second approach, the molecular shape is quantified by the eigen-

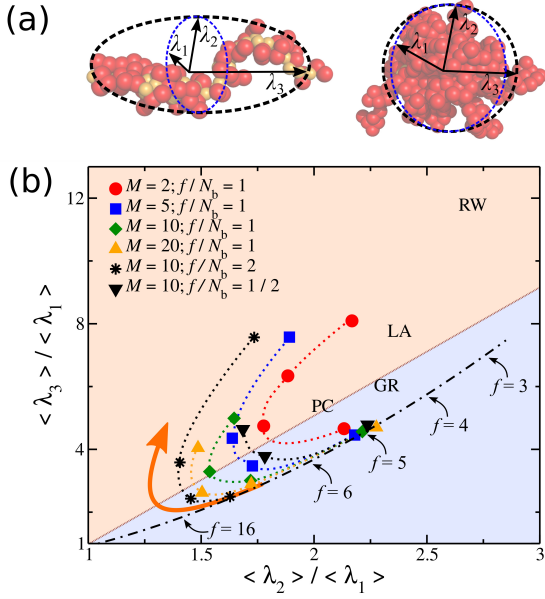


FIG. 11. (a) Schematic illustrating the eigenvalues of radius of gyration for two different bottlebrush polymers, one that has anisotropic shape and one that has relatively spherically symmetric shape. (b) Ratio of the radius of gyration eigenvalues  $\langle \lambda_3 \rangle / \langle \lambda_1 \rangle$  versus  $\langle \lambda_2 \rangle / \langle \lambda_1 \rangle$  for bottlebrush polymers at temperature  $T = 0.5$ . Reference points from Ref. 99 for random walks (RW), lattice animals (LA), percolation clusters (PC), and Gaussian rings (GR) are also presented. The dot-dashed line correspond to a correlation  $\langle \lambda_2 \rangle \sim \sqrt{\langle \lambda_1 \rangle \langle \lambda_3 \rangle}$  for star polymers (see Ref. 31,83) and the small black arrows point along the dot-dashed line the average shape of  $f$ -arms stars. The arrow in orange color highlights the general trend of increasing molecular mass of the bottlebrush polymers. The shaded regions correspond to the tendency of bottlebrush polymers' shape to become more spherical (light blue region) and more anisotropic (light orange) with increasing molecular mass. The boundary between these two regions follows the empirical relation:  $\langle \lambda_3 \rangle \approx \alpha \langle \lambda_2 \rangle + (1 - \alpha) \langle \lambda_1 \rangle$ , where  $\alpha$  is a parameter,  $\alpha \approx 4.3$ .

values of the radius of gyration tensor  $S_p$ . These eigenvalues are denoted below by  $\lambda_1$ ,  $\lambda_2$ , and  $\lambda_3$  and are related to  $R_g^2$  as follows:

$$\text{Tr } S_p = \langle R_g^2 \rangle = \langle \lambda_1 \rangle + \langle \lambda_2 \rangle + \langle \lambda_3 \rangle, \quad (5)$$

where  $\lambda_1 \leq \lambda_2 \leq \lambda_3$  and the brackets  $\langle \rangle$  represent time averages. The eigenvalue data are organized by comparing the two larger eigenvalues with respect to the smallest one. A sphere has  $\langle \lambda_3 \rangle / \langle \lambda_1 \rangle = \langle \lambda_2 \rangle / \langle \lambda_1 \rangle = 1$  and infinite long thin rod has  $\langle \lambda_3 \rangle / \langle \lambda_1 \rangle \rightarrow \infty$  and  $\langle \lambda_2 \rangle / \langle \lambda_1 \rangle$  is finite. For star polymers, the arm length has little impact of the values of these ratios, but an increase in  $f$  leads to molecular conformations of polymers in their melt state range from highly anisotropic structures, as in the case of linear polymers, to relatively symmetric, particle-like structures for large  $f$ , as illustrated in Fig. 11. As discussed in our previous

study,<sup>83</sup> stars having  $f \geq 3$  arms resemble a soft ellipsoid having dimensions that follow a geometric mean, i.e.,  $\langle \lambda_2 \rangle \sim \sqrt{\langle \lambda_1 \rangle \langle \lambda_3 \rangle}$ . For bottlebrush polymers having short backbones, the ratio of the eigenvalues is similar to that of star polymers. For example, the ratios of bottlebrush polymers having  $f/N_b = 1$  is close to the ratios of stars having  $f = 5$  arms, as seen in Fig. 11. Thus, one can assume that bottlebrush polymers with short backbone chain length follow the follow approximately the  $\langle \lambda_2 \rangle \sim \sqrt{\langle \lambda_1 \rangle \langle \lambda_3 \rangle}$ . As the backbone length increases the  $\langle \lambda_3 \rangle / \langle \lambda_1 \rangle$  and  $\langle \lambda_2 \rangle / \langle \lambda_1 \rangle$  ratios decrease, meaning that the bottlebrushes become more spherical, in agreement with calculation of  $\langle R_h \rangle / \langle R_g \rangle$  discussed above. There is a crossover at which this trend is reversed and these ratios start increase for longer backbone lengths, indicating that the overall molecular shape of bottlebrush polymer becomes more anisotropic. This crossover is highlighted in Fig. 11 and follows a relation  $\langle \lambda_3 \rangle \approx \alpha \langle \lambda_2 \rangle + (1 - \alpha) \langle \lambda_1 \rangle$ , where  $\alpha$  is a parameter and based on current results  $\alpha \approx 4.3$ . Curiously, the crossover point in the parameter space nearly coincides with a maximum in  $\langle R_h \rangle / \langle R_g \rangle$ .

## E. Scattering properties of bottlebrush polymers

To probe the structure of bottlebrush polymers, we focus on calculating the spatial correlations between the polymer segments. The static structure factor,  $S(q)$ , is a suitable property for this purpose and describes the mean correlations in the positions of a collection of point particles distributed in space, and  $S(q)$  is defined as:

$$S(q) = \frac{1}{N_s} \left\langle \sum_{j=1}^{N_s} \sum_{k=1}^{N_s} \exp[-i\mathbf{q} \cdot (\mathbf{r}_j - \mathbf{r}_k)] \right\rangle, \quad (6)$$

$$= \frac{1}{N_s} \left\langle \left( \sum_{j=1}^{N_s} \cos \mathbf{q} \cdot \mathbf{r}_j \right)^2 + \left( \sum_{j=1}^{N_s} \sin \mathbf{q} \cdot \mathbf{r}_j \right)^2 \right\rangle \quad (7)$$

where  $i = \sqrt{-1}$ ,  $q = |\mathbf{q}|$  is the wave number,  $\mathbf{r}_j$  is the position of particle  $j$ ,  $\langle \rangle$  denote the time average, and  $N_s$  is the total number of polymer segments defined as  $N_s = N_p(fM + N_b)$ .

### 1. Total structure factor

In the literature of polymer melts, the calculation of  $S(q)$  is often ignored or it is assumed to be similar to the  $S(q)$  of the linear chain analogues. This is not always an accurate premise, however, as seen in Fig. 12. There can be significant differences in  $S(q)$  between different molecular architectures. Bottlebrush polymers have a  $S(q)$  that resembles their linear chain analogues over a wide range  $q$ -values. Specifically,  $S(q)$  exhibits a peak at the characteristic length scales of a segment ( $q\sigma \approx 7$ ) and then as  $q$ -values decrease  $S(q)$  also decreases signifying the suppression of density fluctuations. A small,

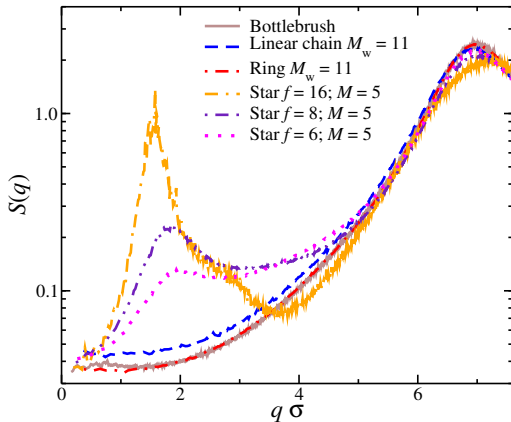


FIG. 12. Full static structure factor  $S(q)$  for different molecular architectures. The results were obtained at temperature  $T = 0.8$ . The bottlebrush system presented here corresponds to a bottlebrush polymer having backbone length  $N_b = 40$ , grafting density  $f/N_b = 1$ , and side chain length  $M = 20$ .

but significant difference between bottlebrush polymer melts and their linear chain analogues is the  $S(q)$  value as  $q \rightarrow 0$  is different between these two molecular architectures. These differences are closely related to the differences in  $\kappa_T$ , defined by Eq. 2. This similarity is natural since  $S(0)$  for an equilibrium fluid is related to  $\kappa_T$  by the sum rule,  $S(0) = \rho k_B T \kappa_T$ .<sup>100</sup> This relationship between the structure and the thermodynamic properties is found to hold for all our polymer systems, providing an important consistency check on the equilibration of our simulations.

Consistent with our findings for the similar  $\kappa_T$  trends for ring and bottlebrush polymers are also the  $S(q)$  trends in the low  $q$ -regime between these two types of molecular architectures. This strong similarity in  $S(q)$  between ring and bottlebrush polymers is striking given that in the example presented in Fig. 12 there is two orders of magnitude difference in molecular mass (rings  $M_w = 11$  and bottlebrush  $M_w = 840$ ). The most notable difference in  $S(q)$  between the molecular architectures is the emergence of an additional peak for highly branched star polymers. An example is presented in Fig. 12 for stars having  $f = 16$  arms and  $M = 5$  at  $T = 0.8$ . The additional peak is due to the high concentration of segments near the core particle and thus effectively corresponds to the average distance between the core particles. This peak becomes noticeable for  $f > 4$  arms, meaning that we anticipate this effect to be observable in bottlebrush polymers having  $f/N_b > 4$  as well. Recent experiments of highly branched bottlebrush polymers exhibit this additional peak at low  $q$ -values supporting our observations.<sup>101</sup>

## 2. Backbone structure factor

We now shift our focus on the static structure factor of the backbone chain segments  $S_b(q)$ , which is calculated by Eq. 7 except that now the set of particles is only the bottlebrush backbone segments. There are two peaks in  $S_b(q)$ . The first peak is located at  $q\sigma \approx 7.5$ , corresponding to spatial correlations between neighboring and/or bonded segments along the bottlebrush backbone. The second peak, which we term as “primary peak”, is our main focus below. This primary peak is located at smaller values of  $q$ , i.e., at larger distances since  $q = 2\pi/r$  and it characterizes the average distance between neighboring backbones. The height of the primary peak becomes more pronounced for bottlebrush polymers having longer side chains, as seen in Fig. 13a, and bottlebrushes having higher grafting density along the backbone, not shown here. We interpret this behavior as the deriving from a soft polymeric corona surrounding the backbone, which effectively localizes the backbones at length scales associated with the peak location by repelling neighboring bottlebrush backbones. The primary peak shifting to smaller  $q$ -values as  $M$  increases, because  $M$  controls the size of this soft polymeric corona and as a result  $M$  influences the average interchain distance.

The emergence of these structural features is reminiscent of the rise of particle-like structural characteristics of highly branched star polymers in solution, where the ability to control these structural correlations in solutions of star polymers by the variation of molecular structure alone have stimulated the polymer community in previous decades.<sup>102,103</sup> It has been suggested that the structural features of highly branched star polymers are preserved in the crossover from solution to a melt state.<sup>69,104</sup> Indeed, the structure factor of the core particles  $S_c(q)$  of star polymers in the melt state exhibit particle-like features, as illustrated in Fig. 13b; the full  $S(q)$  is presented in Fig. 12. The peak in  $S_c(q)$  coincides with the peak observed in  $S(q)$  at the lower  $q$  regime, meaning that the primary peak in highly branched polymer melts not the average intermolecular distance but also the fact that the polymer segments are not uniformly distributed in the material. This variation in local density contributes to the heterogeneous dynamics that highly branched stars exhibit.<sup>69,105</sup> A similar control of the structure through the variation of molecular architecture can be archived with polymer-grafted nanoparticles in solution/polymer matrix<sup>106,107</sup> and in the absence of solvent,<sup>108–113</sup> and with dendrimers.<sup>79,114</sup>

By comparing the structural correlations for bottlebrush, linear chains, and star polymers together, as illustrated in Fig. 13, we can make the following observations. Linear chains in the melt state exhibit no correlations for a wide range of length scales, though there is a suppression of density fluctuations at length scales larger than the size of the polymer chain, this lack of structural correlations has made the linear chains to be considered as ‘ultra soft’ particles.<sup>115</sup> Low  $f$  star poly-

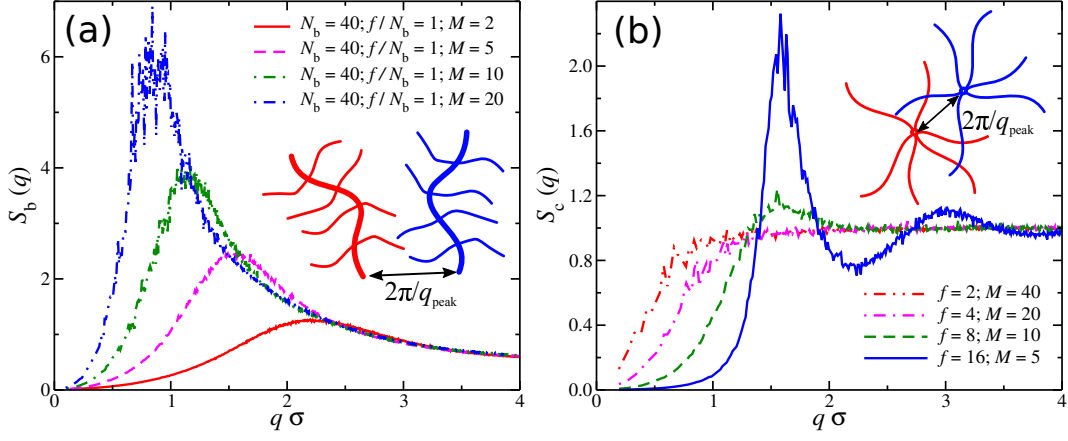


FIG. 13. (a) Structure factor of bottlebrush backbone chain segments  $S_b(q)$ . (b) Structure factor of core particles  $S_c(q)$  in star polymer melts having molecular mass  $M_w = 81$ . The results were obtained at temperature  $T = 0.8$ .

mers, having same  $M_w$  as in the case of linear chains, suppresses the density fluctuations at higher  $q$ -values as the molecular size is decreased and no other structural correlations emerge similar to the case of linear chain polymer melts. A structural peak starts to emerge at length scales of the order of the intermolecular distance for  $f \gtrsim 6$ . This is also the same number of arms at which a configurational transition from highly anisotropic linear chains to highly symmetric particle-like star polymers occurs.<sup>31,116</sup> The colloidal/spherical-like structural correlations are evident for stars having  $f = 16$ , as illustrated in Fig. 13b. Analogous observations can be made for bottlebrush polymers in the melt state. The average distance between the backbones increases with increasing  $M$ . This is understandable since the length of the side chains greatly influences the size polymeric corona. This localization of the backbone indicates the emergence of intramolecular heterogeneous dynamics<sup>69</sup> which are symptomatic to non-trivial behaviors, such as thermal jamming.<sup>110,117</sup> However, the primary peak becomes narrower and its height increases as  $M$  increases, as illustrated in Fig. 13a, suggesting that the backbones also localize at the center of their own polymeric corona. To better understand these results we examine the mass scaling of the location of the primary peak in bottlebrush polymers.

We track the location of the primary peak in  $S(q)$  and the results are presented in Fig. 14. For long enough backbone chain lengths ( $N_b \geq 20$ ), the location of the primary peak in  $S_b(q)$  is the same irrespective of  $N_b$  and  $M$ . This effect is also clearly illustrated at the inset of Fig. 14. Moreover, the location of the peak scales with  $M$  as  $q_{\text{peak}} \sim M^{-\mu}$ , where  $\mu$  is exponent that reflects the nature of packing between the neighboring bottlebrush backbones. For  $N_b \geq 20$ ,  $\mu \approx 0.4$ , which indicates an intermediate scaling between the particle scaling of  $1/3$  and linear chain mesh of  $1/2$ . For short backbone chain lengths ( $N_b < 20$ ) this scaling gradually changes to  $q_{\text{peak}} \sim M^{-1/3}$ , which corresponds to a particle-like

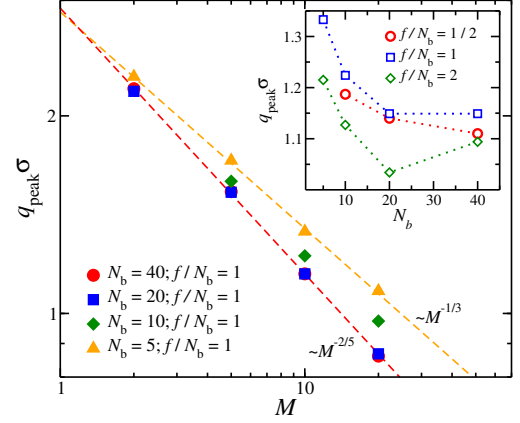


FIG. 14. Location of the primary peak  $q_{\text{peak}}$  in the structure factor of the bottlebrush backbone chain segments  $S_b(q)$  as a function of the side-chain length  $M$ . Results for different backbone chain lengths  $N_b$  are also presented. The dashed lines are guides for the eye. (Inset)  $q_{\text{peak}}$  for bottlebrush polymers having  $M = 10$  as a function of  $N_b$  at different grafting densities  $f/N_b = 1/2, 1, \text{ and } 2$ .

scaling; we note that for star polymer in the melt state, we find a mass scaling exponent of  $-1/3$ , as expected. This type of crossover is not surprising and has been typically observed in polyelectrolyte solutions,<sup>118–123</sup> where at low concentrations polyelectrolyte chains act as individual particles and as polymer concentration increases the scaling gradually changes to  $1/2$ . In our case, an increase in  $M$  results in an effective “dilution” of the backbone concentration. However, for the molecular parameters in our study, we do not find evidence of a  $1/2$  scaling.

We briefly discuss the effect of the grafting density along the bottlebrush backbone on  $q_{\text{peak}}$ . In particular, we focus on bottlebrush polymers having  $M = 10$  and the results are presented in the inset of Fig. 14.

For  $f/N_b = 1/2$  and 1,  $q_{\text{peak}}$  decreases as  $N_b$  increases, suggesting that the average distance between backbones increases for longer length backbones. For  $f/N_b = 1$ , the location of the primary peak remains the same for  $N_b = 20$  and 40, suggesting that either there is a plateau or a minimum for  $20 < N_b < 40$ . The latter is probable because a minimum is observed in the case of  $f/N_b = 2$  as it is illustrated at the inset of Fig. 14. We note that the minimum occurs for molecular parameters that exhibit a maximum in  $\langle R_h \rangle / \langle R_g \rangle$ . In other words, the average distance between backbones, as determined by  $q_{\text{peak}}$ , is for bottlebrush polymers having nearly spherical molecular conformation. Future work will focus on testing these observations to gain deeper insights on the effects of grafting density along the bottlebrush backbone on the structure and other material properties.

### 3. Bottlebrush and backbone form factor

We briefly examine the structure of the bottlebrush polymers at length scales smaller than  $R_g$ . First, we calculate the form factor  $P(q)$  for bottlebrush polymers and compare it with the form factor of the corresponding backbone chains, see Fig. 15.  $P(q)$  is nearly the same whether the whole polymer (backbone and side chains) or just the backbone chain is considered for bottlebrush polymer having  $f/N_b = 1/2$  and for  $q\sigma > 2\pi/R_g$  as illustrated in Fig. 15. Moreover,  $P(q)$  scales as  $P(q) \sim q^{-1.6}$  for  $q\sigma > 2\pi/R_g$ , indicating that the backbone chain has a structure that lies between a rod ( $P(q) \sim q^{-1}$ ) and a Gaussian chain  $P(q) \sim q^{-2}$ . Increasing  $f/N_b$  leads to stretching the backbone chain due to the excluded volume interaction between the side chains as we discussed above. The effect of this stretching is reflected in  $P(q)$  of the backbone chains with  $P(q) \sim q^{-1.2}$ , where the scaling is closer to rod-like behavior. Curiously, the scaling of the form factor of the whole bottlebrush polymer was unaffected by  $f/N_b$  variation. Additionally, for  $M = 10$  and  $f/N_b = 1$ , we find there is no significant changes in the scaling of the form factor with  $q$ .

### F. General Observations

Bottlebrush polymers having  $f/N_b = 1$  exhibit three distinct regimes. Bottlebrush polymers having  $N_b < M$  are rather similar to star polymers, both in terms of molecular shape and molecular packing as determined from scattering  $q_{\text{peak}} \sim M^{-1/3}$ . In this regime the conformational properties are predominately determined by the side chains, while the backbone plays little role. We may then call this regime as ‘many-arm star’ due to the strong similarities found in this regime. The second regime corresponds to bottlebrush polymers having  $N_b \approx M$ , at this regime the molecular shape of the bottlebrush polymers becomes more spherically symmetric. From scattering of the backbone chain seg-

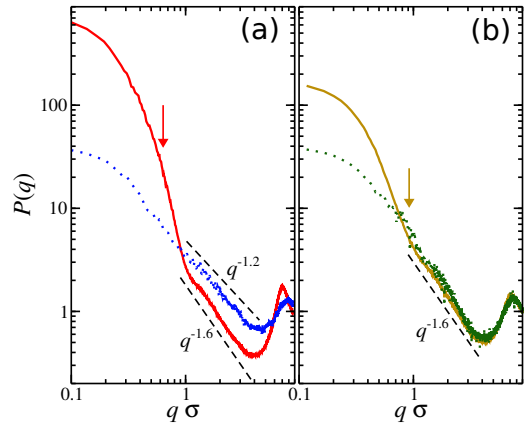


FIG. 15. The form factor  $P(q)$  of bottlebrush polymers (continuous line) having different grafting densities: (a)  $f/N_b = 2$  and (b)  $f/N_b = 1/2$  in melt conditions at temperature  $T = 0.8$ . The backbone chains (dotted line) are also presented. The arrows mark the average radius of gyration of the whole bottlebrush polymer  $\langle R_g \rangle$  and the dashed lines are guides for the eye.

ments we find a crossover from  $\nu = 1/3$  to  $2/5$ . The third regime corresponds to bottlebrush polymers having  $N_b \gg M$ . The molecular shape becomes more anisotropic and  $q_{\text{peak}} \sim M^{-2/5}$ . An overview of these results are presented in Fig. 16.

We also briefly summarize the results found for the mass scaling of bottlebrush polymers. In the literature, it is typical to present the mass scaling of a bottlebrush polymer  $R_g \sim M_w^\nu$  and increase  $M_w$  by increasing  $N_b$  while keeping  $f/N_b$  and  $M$  fixed. Based on this approach, we observe a crossover behavior from  $\nu = 1/3$  for short backbone lengths to a higher value of  $\nu$ ; the exact value cannot be determined with the current results but we expect to be no larger than  $1/2$  for  $N_b \gg M$ . If the same  $R_g$  results are analyzed by increasing  $M_w$  differently, i.e., by increasing  $M$  while keeping  $f/N_b$  and  $N_b$  fixed, then we obtain consistent power-law relations, i.e.,  $\langle R_g \rangle \sim M_w^\nu$  and  $\nu$  exhibits considerable dependence on  $N_b$ . Specifically we find that  $\nu \approx 1/2$  for  $N_b = 5$  and as the backbone chain length increases  $\nu$  decreases for  $N_b = 40$  we find the apparent mass scaling exponent  $\nu \approx 0.28$ .

Finally, we outline our observations on the thermodynamic behavior of bottlebrush polymer melts. We find that bottlebrush polymers in the melt state exhibit a packing efficiency on a segmental scale that is similar to the ring polymers and stars having a moderate number of arms  $f \approx 5$  to 6. Similar trends are found in the derivative properties that is the isobaric thermal expansion coefficient and isothermal compressibility. These material properties are important for the design of materials for 3-D printing and polymer processing, and thus illustrate the importance of thermodynamics in the description and characterization of polymer melts having

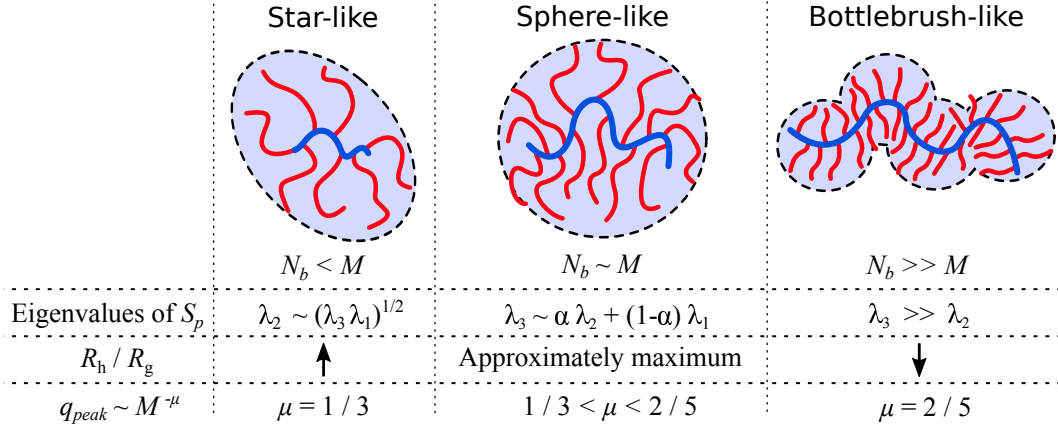


FIG. 16. Schematic illustrating an overview of the various trends in conformation (eigenvalues of the radius of gyration tensor  $S_p$  and the ratio of the hydrodynamic radius over the radius of gyration  $R_h/R_g$ ) and the scaling of the primary peak in the structure factor of bottlebrush polymers in melt conditions. The results are organized based on three regimes.

different molecular architectures.

## V. CONCLUSIONS

In this work, computer simulations of a thermodynamically consistent bead-spring model have been used to gain insights into the thermodynamic, conformational, and structural properties of bottlebrush polymer melts. The study was motivated by the unique physical properties of bottlebrush polymer melts and the desire to describe their properties with respect to other known molecular architectures such as star and ring polymers. Through this comparison we found that bottlebrush polymer melts exhibit trends in thermodynamic properties, specifically in segmental density, isothermal compressibility, and isobaric thermal expansion, quantitatively similar to ring polymer melts and star polymer melts having  $f = 5$  to 6 arms. These similarities extend in the mass scaling of the radius of gyration and hydrodynamic radius. An analysis of the eigenvalues of radius of gyration further indicate that the average molecular shape of bottlebrush polymers changes significantly with molecular topology. Specifically, we find that the average shape of bottlebrush polymers having short backbone chains with respect to side chain length tend to have on average an ellipsoidal shape, which is characteristic of star polymers in the melt state. Once the side chain length become comparable to backbone length then the overall molecular shape becomes more spherically symmetric. When the backbone chain becomes longer than the side chain length then the bottlebrush polymers become more anisotropic as expected. Finally, we calculate the static structure factor of the backbone segments and we find the emergence of a peak at length scales that characterize the average distance between the backbone chain. This peak is absent when we calculate the full segment static structure factor. We

characterize the scaling of this peak with variation of the parameters of the bottlebrush molecular architecture.

One of the unresolved issues is how the structure and packing of bottlebrush polymers changes upon going from dilute solution to the polymer melt state. Both simulations and experiments indicate that ring polymers exhibit mass scaling exponents governing size, dynamics, etc., similar to linear chains when the polymers are diluted in a good solvent. However, ring polymers in the melt exhibit compact conformations similar to randomly branched polymers in the melt state.<sup>47,69</sup> We have recently shown<sup>69</sup> that star polymers having a moderate number of arms seem to follow a similar pattern of behavior and the present work, indicating that bottlebrush polymers also more resemble randomly branched polymers in the melt state than linear chains. We expect, based on our previous work on star and ring polymers, that bottlebrush polymers in dilute solutions should exhibit a swollen geometry with similarities to linear chain polymers in good solvents so that a significant change in polymer conformation should occur with increasing bottlebrush polymer concentration. This expectation remains to be tested by simulation and by experiment.

Our finding of a strong similarity between bottlebrush polymers, and other branched polymer exhibiting large fluctuation in conformational shape, to the configurational properties of randomly branched polymers in the melt state would seem to indicate that our results should also be relevant to understanding the material properties of other types of branched polymer materials. For example, common commodity polymers in the melt state, such as alkanes, often involve random branching of the molecules in their synthesis.<sup>124–127</sup> We also note that the supercoiled DNA in the chromosomes of bacteria and other organisms has been observed to have a randomly branched polymer structure<sup>128–130</sup> so that the emergence of chromosome territories separating

DNA molecules under crowded conditions of the cell under interphase conditions (non-replicating genetic conditions) could be a natural consequence of the randomly branched polymer structure of these macromolecules. In summary, we may expect numerous practical consequences arising from the alteration of molecular packing from the presence of molecular branching in polymer materials. We plan to explore these other classes of branched macromolecules in the future.

## ACKNOWLEDGMENTS

We gratefully acknowledge the support of the NIST Director's Office through the NIST Fellows' postdoctoral grants program. Official contribution of the U.S. National Institute of Standards and Technology.

- <sup>1</sup>S. Lee and N. D. Spencer, *Science* **319**, 575 (2008).
- <sup>2</sup>H. Xu, F. C. Sun, D. G. Shirvanyants, M. Rubinstein, D. Shabratov, K. L. Beers, K. Matyjaszewski, and S. S. Sheiko, *Adv. Mater.* **19**, 2930 (2007).
- <sup>3</sup>G. M. Miyake, V. A. Piunova, R. A. Weitekamp, and R. H. Grubbs, *Angew. Chem. Int. Ed.* **51**, 112246 (2012).
- <sup>4</sup>G. M. Miyake, R. A. Weitekamp, V. A. Piunova, and R. H. Grubbs, *J. Am. Chem. Soc.* **134**, 14249 (2012).
- <sup>5</sup>B. R. Sveinbjörnsson, R. A. Weitekamp, G. M. Miyake, Y. Xia, H. A. Atwater, and R. H. Grubbs, *Proc. Natl. Acad. Sci. U.S.A.* **109**, 14332 (2012).
- <sup>6</sup>A. Nese, N. V. Lebedeva, G. Sherwood, S. Averick, Y. Li, H. Gao, L. Peteanu, S. S. Sheiko, and K. Matyjaszewski, *Macromolecules* **44**, 5905 (2011).
- <sup>7</sup>T. Pakula, Y. Zhang, K. Matyjaszewski, H. i. Lee, H. Boerner, S. Qin, and G. C. Berry, *Polymer* **47**, 7198 (2006).
- <sup>8</sup>J. M. Sarapas, E. P. Chan, E. M. Rettner, and K. L. Beers, *Macromolecules* **51**, 2359 (2018).
- <sup>9</sup>J. Bolton, T. S. Bailey, and J. Rzayev, *Nano Lett.* **11**, 998 (2010).
- <sup>10</sup>J. Rzayev, *ACS Macro Lett.* **1**, 1146 (2012).
- <sup>11</sup>A. Chremos and P. E. Theodorakis, *ACS Macro Lett.* **3**, 1096 (2014).
- <sup>12</sup>R. Verduzco, X. Y. Li, S. L. Pesek, and G. E. Stein, *Chem. Soc. Rev.* **44**, 2405 (2015).
- <sup>13</sup>A. Chremos and P. E. Theodorakis, *Polymer* **97**, 191 (2016).
- <sup>14</sup>A. Kano, T. Yamano, S. W. Choi, and A. Maruyama, *Adv. Mater. Res.* **47–50**, 762 (2008).
- <sup>15</sup>K. L. Beers, S. G. Gaynor, K. Matyjaszewski, S. S. Sheiko, and M. Möller, *Macromolecules* **31**, 9413 (1998).
- <sup>16</sup>N. Hadjichristidis, M. Pitsikalis, S. Pispas, and H. Iatrou, *Chem. Rev.* **101**, 3747 (2001).
- <sup>17</sup>S. Jha, S. Dutta, and N. B. Bowden, *Macromolecules* **37**, 4365 (2004).
- <sup>18</sup>Z. Li, K. Zhang, J. Ma, C. Cheng, and K. L. Wooley, *J. Polym. Sci. A Polym. Chem.* **47**, 5557 (2009).
- <sup>19</sup>S. L. Pesek, X. Li, B. Hammouda, K. Hong, and R. Verduzco, *Macromolecules* **46**, 6998 (2013).
- <sup>20</sup>D. Neugebauer, Y. Zhang, T. Pakula, S. S. Sheiko, and K. Matyjaszewski, *Macromolecules* **36**, 6746 (2003).
- <sup>21</sup>S. J. Daslin, M. A. Hillmyer, and F. S. Bates, *ACS Macro Lett.* **3**, 423 (2014).
- <sup>22</sup>C. M. Bates, A. B. Chang, N. Momčilović, S. C. Jones, and R. H. Grubbs, *Macromolecules* **48**, 4967 (2015).
- <sup>23</sup>C. R. Lopez-Baron, P. Brant, and A. P. Eberle, *J. Rheol.* **59**, 865 (2015).
- <sup>24</sup>S. J. Daslin, M. A. Hillmyer, and F. S. Bates, *Macromolecules* **48**, 4680 (2015).
- <sup>25</sup>W. F. M. Daniel, J. B. M. Vatankhah-Varnoosfaderani, K. Matyjaszewski, J. Paturej, M. Rubinstein, and A. V. D. S. S. Sheiko, *Nat. Mater.* **15**, 183 (2015).
- <sup>26</sup>C. M. Bates, A. B. Chang, M. W. Schulze, N. Momčilović, S. C. Jones, and R. H. Grubbs, *J. Polym. Sci. B* **54**, 292 (2016).
- <sup>27</sup>S. L. Pesek, Q. Xiang, B. Hammouda, and R. Verduzco, *J. Pol. Sci.* **55**, 104 (2017).
- <sup>28</sup>P. E. Theodorakis, H. P. Hsu, P. Paul, and K. Binder, *J. Chem. Phys.* **135**, 164903 (2011).
- <sup>29</sup>J. Paturej, S. S. Sheiko, S. Panyukov, and M. Rubinstein, *Science Advances* **2**, e1601478 (2016).
- <sup>30</sup>J. Zhang, T. Li, A. M. Mannion, and D. K. Schneiderman, *ACS Macro Lett.* **5**, 407 (2016).
- <sup>31</sup>A. Chremos and J. F. Douglas, *J. Chem. Phys.* **143**, 111104 (2015).
- <sup>32</sup>P. J. Flory, *Statistical Mechanics of Chain Molecules* (Interscience, New York, 1969).
- <sup>33</sup>T. C. Lubensky and J. Isaacson, *Phys. Rev. A* **20**, 2130 (1979).
- <sup>34</sup>B. Li, N. Madras, and A. D. Sokal, *J. Stat. Phys.* **80**, 661 (1995).
- <sup>35</sup>M. Wittkop, S. Kreitmeier, D., and Göritz, *J. Chem. Phys.* **104**, 3373 (1996).
- <sup>36</sup>K. F. Freed, *J. Chem. Phys.* **79**, 6357 (1983).
- <sup>37</sup>J. A. M. Smit, J. A. P. P. Van Dijk, M. G. Mennen, and M. Daoud, *J. Chem. Phys.* **25**, 3585 (1992).
- <sup>38</sup>E. Bouchaud, M. Delsanti, M. Adam, M. Daoud, and D. Durand, *J. Phys. France* **47**, 1273 (1986).
- <sup>39</sup>J. F. Douglas, *Phys. Rev. E* **54**, 2677 (1996), The scaling exponent  $\nu$  for polymer without excluded volume is  $\nu = 1/4$  and it is not equivalent to branched polymers at their  $\theta$ -point or having screened excluded volume interactions where  $\nu \approx 2/5$ . "Percolation clusters" are branched polymers with screened excluded volume interactions.
- <sup>40</sup>T. P. Lodge and M. Muthukumar, *J. Phys. Chem.* **100**, 13275 (1996).
- <sup>41</sup>B. J. Sung and A. Yethiraj, *J. Chem. Phys.* **138**, 234904 (2013).
- <sup>42</sup>P. Polanowski, J. K. Jeszka, and A. Sikorski, *Macromolecules* **47**, 4830 (2014).
- <sup>43</sup>M. Dolgushev, A. L. Hauder, P. Pelagejcev, and J. P. Wittmer, *Phys. Rev. E* **96**, 012501 (2017).
- <sup>44</sup>A. Rosa and R. Everaers, *Soft Matter* **145**, 164906 (2016).
- <sup>45</sup>R. Everaers, A. Y. Grosberg, M. Rubinstein, and A. Rosa, *Soft Matter* **13**, 1223 (2017).
- <sup>46</sup>A. Rosa and R. Everaers, *Phys. Rev. E* **95**, 012117 (2017).
- <sup>47</sup>S. Y. Reigh and D. Y. Yoon, *ACS Macro Lett.* **2**, 296 (2013).
- <sup>48</sup>J. Cardy, *Journal of Physics A* **34**, L665 (2001).
- <sup>49</sup>E. J. Van Rensburg, *The statistical mechanics of interacting walks, polygons, animals and vesicles* (Oxford Lecture Series in Mathe., Oxford, 2015).
- <sup>50</sup>J. F. Douglas, T. Ishinabe, A. M. Nemirovsky, and K. F. Freed, *J. Phys. A* **26**, 1835 (1992).
- <sup>51</sup>J. F. Douglas, B. J. Cherayil, and K. F. Freed, *Macromolecules* **18**, 2455 (1985).
- <sup>52</sup>G. Parisi, *Phys. Lett.* **81B**, 357 (1979).
- <sup>53</sup>B. Durhuus, T. Fröhlich, and T. Jonsson, *Nucl. Phys. B* **257**, 779 (1985).
- <sup>54</sup>D. V. Boulatov, V. A. Kazakov, I. K. Kostov, and A. A. Migdal, *Nucl. Phys. B* **275**, 641 (1986).
- <sup>55</sup>A. L. Stella, E. Orlandini, I. Beichl, F. Sullivan, M. C. Tesi, and T. L. Einstein, *Phys. Rev. Lett.* **69**, 3650 (1992).
- <sup>56</sup>B. H. Zimm and W. H. Stockmayer, *J. Chem. Phys.* **17**, 1301 (1949).
- <sup>57</sup>M. Daoud, P. Pincus, W. H. Stockmayer, and T. Witten, *Macromolecules* **16**, 1833 (1983).
- <sup>58</sup>D. Dhar, *Phys. Rev. Lett.* **51**, 853 (1983).
- <sup>59</sup>M. Adam, M. Delsanti, J. P. Munch, and D. Durand, *J. Phys. France* **48**, 1809 (1987).
- <sup>60</sup>L. J. Fetters, D. J. Lohse, D. Richter, T. A. Witten, and A. Zirkel, *Macromolecules* **27**, 4639 (1994).
- <sup>61</sup>M. Kapnistos, M. Lang, D. Vlassopoulos, W. Pyckhout-Hintzen, D. Richter, D. Cho, T. Chang, and M. Rubinstein, *Nat. Mater.* **7**, 997 (2008).

- <sup>62</sup>W. Lo and M. S. Turner, *EPL* **102**, 58005 (2013).
- <sup>63</sup>M. Z. Slimani, P. Bacova, M. Bernabei, A. Narros, C. N. Likos, and A. J. Moreno, *ACS Macro Lett.* **3**, 611 (2014).
- <sup>64</sup>G. Liu, X. Feng, K. Lang, R. Zhang, D. Guo, S. Yang, and S. Z. Cheng, *Macromolecules* **50**, 6637 (2017).
- <sup>65</sup>A. Chremos and J. F. Douglas, *Annalen der Physik* **529**, 1600342 (2017).
- <sup>66</sup>S. J. Plimpton, *J. Comput. Phys.* **117**, 1 (1995).
- <sup>67</sup>R. S. Hoy, K. Foteinopoulou, and M. Kröger, *Phys. Rev. E* **80**, 031803 (2009).
- <sup>68</sup>K. Hur, R. G. Winkler, and D. Y. Yoon, *Macromolecules* **39**, 3975 (2006).
- <sup>69</sup>A. Chremos, E. Glynos, and P. F. Green, *J. Chem. Phys.* **142**, 044901 (2015).
- <sup>70</sup>M. Hilbert, *Phase Equilibria, Phase Diagrams and Phase Transformations* (Cambridge University Press, Cambridge, 2008).
- <sup>71</sup>Z. Dobkowski, *Eur. Polym. J.* **18**, 563 (1982).
- <sup>72</sup>A. Bormuth, P. Henritzi, and M. Vogel, *Macromolecules* **43**, 8985 (2010).
- <sup>73</sup>J. B. Hubbard and J. F. Douglas, *Phys. Rev. E* **47**, 2983 (1993).
- <sup>74</sup>M. L. Mansfield, J. F. Douglas, and E. J. Garboczi, *Phys. Rev. E* **64**, 061401 (2001).
- <sup>75</sup>D. Juba, D. J. Audus, M. Mascagni, J. F. Douglas, and W. Keyrouz, *Journal of Research of National Institute of Standards and Technology* **122**, doi:10.6028/jres.122.020 (2017).
- <sup>76</sup>P. G. de Gennes, *Scaling Concepts in Polymer Physics* (Cornell University Press, Ithaca, 1979).
- <sup>77</sup>M. Rubinstein and R. H. Colby, *Polymer Physics* (Oxford University Press, Oxford, 2003).
- <sup>78</sup>V. Arrghi, S. Gagliardi, A. C. Dagger, J. A. Semlyen, J. S. Higgins, and M. J. Shenton, *Macromolecules* **37**, 8057 (2004).
- <sup>79</sup>F. Mallamace, E. Canetta, D. Lombardo, A. Mazzaglia, A. R. L. M. Scolaro, and G. Maino, *Physica A* **304**, 235 (2002).
- <sup>80</sup>C. N. Likos, M. Schmidt, H. Löwen, M. Ballauff, D. Pötschke, and P. Lindner, *Macromolecules* **34**, 2914 (2001).
- <sup>81</sup>C. N. Likos, S. Rosenfeldt, N. Dingenouts, M. Ballauff, P. Lindner, N. Werner, and F. Vögtle, *J. Chem. Phys.* **117**, 1869 (2002).
- <sup>82</sup>K. Karatasos, *Macromolecules* **38**, 4472 (2005).
- <sup>83</sup>A. Chremos, C. Jeong, and J. F. Douglas, *Soft Matter* **13**, 5778 (2017).
- <sup>84</sup>K. F. Freed and S. F. Edwards, *J. Chem. Phys.* **61**, 3626 (1974).
- <sup>85</sup>H. P. Hsu, W. Paul, and K. Binder, *Macromolecules* **43**, 3094 (2010).
- <sup>86</sup>H. P. Hsu, W. Paul, and K. Binder, *Polymer Science Series C* **55**, 39 (2013).
- <sup>87</sup>J. Paturej and T. Kreer, *Soft matter* **13**, 8534 (2017).
- <sup>88</sup>I. N. Haugan, M. J. Maher, A. B. Chang, T. P. Lin, R. H. Grubbs, M. A. Hillmyer, and F. S. Bates, *ACS Macro Lett.* **7**, 525 (2018).
- <sup>89</sup>B. E. Eichinger, *Macromolecules* **10**, 671 (1977).
- <sup>90</sup>J. Mazur, C. M. Gutman, and F. L. McCrackin, *Macromolecules* **6**, 872 (1973).
- <sup>91</sup>K. Šolc, *Macromolecules* **6**, 378 (1973).
- <sup>92</sup>J. F. Douglas, J. Roovers, and K. F. Freed, *Macromolecules* **23**, 4168 (1990).
- <sup>93</sup>M. Bishop, J. H. R. Clarke, A. Rey, and J. J. Freie, *J. Chem. Phys.* **94**, 4009 (1991).
- <sup>94</sup>A. Forni, F. Ganazzoli, and M. Vacatello, *Macromolecules* **30**, 4737 (1997).
- <sup>95</sup>M. L. Mansfield and J. F. Douglas, *Condens. Matter Phys.* **5**, 249 (2002).
- <sup>96</sup>O. Jagodzinski, E. Eisenriegler, and K. Kremer, *J. Phys. I* (France) **2**, 2243 (1992).
- <sup>97</sup>K. Hur, C. Jeong, R. G. Winkler, N. Laceyvic, R. H. Gee, and D. Y. Yoon, *Macromolecules* **44**, 2311 (2011).
- <sup>98</sup>M. L. Mansfield and J. F. Douglas, *Macromolecules* **41**, 5422 (2008).
- <sup>99</sup>M. L. Mansfield and J. F. Douglas, *J. Chem. Phys.* **139**, 044901 (2013).
- <sup>100</sup>J.-P. Hansen and I. R. McDonald, *Theory of simple liquids* (Academic Press, Cambridge, 2006).
- <sup>101</sup>C. López-Barrón, A. H. Tsou, J. M. Younker, A. I. Norman, J. J. Schaefer, J. R. Hagadorn, and J. A. Throckmorton, *Macromolecules* p. 10.1021/acs.macromol.7b02524 (2018).
- <sup>102</sup>C. N. Likos, H. Löwen, M. Watzlawek, B. Abbas, O. Jucknischke, J. Allgaier, and D. Richter, *Phys. Rev. Lett.* **80**, 4450 (1998).
- <sup>103</sup>C. N. Likos, *Soft Matter* **2**, 478 (2006).
- <sup>104</sup>T. Pakula, *Comput. Theor. Polym. Sci.* **8**, 21 (1998).
- <sup>105</sup>C. H. Adams, M. G. Brereton, L. R. Hutchings, P. G. Klein, T. C. B. McLeish, R. W. Richards, and M. E. Ries, *Macromolecules* **33**, 7101 (2000).
- <sup>106</sup>S. Goyal and F. A. Escobedo, *J. Chem. Phys.* **135**, 184902 (2011).
- <sup>107</sup>A. Jayaraman and K. S. Schweizer, *Macromolecules* **42**, 8423 (2009).
- <sup>108</sup>H.-Y. Yu and D. L. Koch, *Langmuir* **26**, 16801 (2010).
- <sup>109</sup>A. Chremos, A. Z. Panagiotopoulos, H.-Y. Yu, and D. L. Koch, *J. Chem. Phys.* **135**, 114901 (2011).
- <sup>110</sup>A. Chremos and A. Z. Panagiotopoulos, *Phys. Rev. Lett.* **107**, 105503 (2011).
- <sup>111</sup>H.-Y. Yu and D. L. Koch, *J. Rheol.* **58**, 369 (2014).
- <sup>112</sup>N. J. Fernandes, H. Koerner, E. P. Giannelis, and R. A. Vaia, *MRS Commun.* **3**, 13 (2013).
- <sup>113</sup>S. Srivastava, J. L. Schaefer, Z. Yang, Z. Tu, , and L. A. Archer, *Advanced Materials* **26**, 201 (2014).
- <sup>114</sup>H. M. Harreis, C. N. Likos, and M. Ballauff, *J. Chem. Phys.* **118**, 1979 (2003).
- <sup>115</sup>A. A. Louis, P. G. Bolhuis, J. P. Hansen, and E. J. Meijer, *Phys. Rev. Lett.* **85**, 2522 (2000).
- <sup>116</sup>A. Chremos and J. F. Douglas, *Soft Matter* **12**, 9527 (2016).
- <sup>117</sup>P. Agarwal, M. Chopra, and L. A. Archer, *Angew. Chem. Int. Ed.* **50**, 8670 (2011).
- <sup>118</sup>P. G. de Gennes, P. Pincus, F. Brochard, and R. M. Velasco, *J. Phys. (Paris)* **37**, 1461 (1976).
- <sup>119</sup>L. Wang and V. A. Bloomfield, *Macromolecules* **24**, 5791 (1991).
- <sup>120</sup>E. E. Maier, R. Krause, M. Deggelmann, M. Hagenbuchle, and R. Weber, *Macromolecules* **25**, 1125 (1992).
- <sup>121</sup>A. Yethiraj and C.-Y. Shew, *Phys. Rev. Lett.* **77**, 3937 (1996).
- <sup>122</sup>A. Yethiraj, *Phys. Rev. Lett.* **78**, 3789 (1997).
- <sup>123</sup>A. Chremos and J. F. Douglas, *J. Chem. Phys.* **147**, 044906 (2017).
- <sup>124</sup>D. J. Read and J. B. Soares, *Macromolecules* **36**, 10037 (2003).
- <sup>125</sup>H. Tobita, *J. Pol. Science* **39**, 391 (2000).
- <sup>126</sup>C. Das, D. J. Read, J. M. Soulages, and P. P. Shrirodkar, *Macromolecules* **47**, 5860 (2014).
- <sup>127</sup>C. Das, D. J. Read, J. M. Soulages, and P. P. Shrirodkar, *Macromol. Theory Simul.* **26**, 1700006 (2017).
- <sup>128</sup>A. V. Vologodskii, S. D. Levene, K. V. Klenin, M. Frank-Kamenetskii, and N. R. Cozzarelli, *J. Mol. Biol.* **227**, 1224 (1992).
- <sup>129</sup>J. F. Marko and E. D. Siggia, *Phys. Rev. E* **52**, 2912 (1995).
- <sup>130</sup>S. H. Hong, E. Toro, K. I. Mortensen, M. A. D. de la Rosa, S. Doniach, L. Shapiro, A. J. Spakowitz, and H. H. McAdams, *Proc. Natl. Acad. Sci. U.S.A.* **110**, 1674 (2013).